Design and Analysis of a Human Powered Vehicle's Frame and Seat Assistance Mechanism

by

Bradley S. Helm

A Report Submitted to the Faculty of the

Milwaukee School of Engineering

in Partial Fulfillment of the

Requirements for the Degree of

Master of Science in Engineering

Milwaukee, Wisconsin

February 2017

ABSTRACT

The objective of this project was to complete the redesign and analysis of a human powered vehicle (HPV) called the Heliocycle, which is an existing tricycle (also referred to as trike). The Heliocycle was a Senior Design Project that was completed at the Milwaukee School of Engineering (MSOE) by Bradley Helm, Kelly Bauserman, Michael Caelwaerts, and Nicholas Weis from September 2014 through May 2015. Since the Heliocycle's debut in May 2015, it has been showcased and ridden, gaining exposure and feedback. In addition, a company (Omnium Cycles, LLC) was formed around the Heliocycle, and the Heliocycle received a provisional patent. This redesign was completed to improve the original design, based on knowledge gained through fabricating the initial prototype and feedback gathered during showcases. A brief market analysis determined a need for this trike and defined the target audience who would be most likely to buy and use this product.

In order to complete this project, a five-stage design process was followed. Throughout these stages, this project involved engineering design and analysis, which included the selection of materials, mechanics of materials, and finite element analysis, as well as some minor business aspects. The analysis was completed to confirm the design would be safe and withstand the stated maximum load established during the design. There was communication with the potential fabrication team (FT) to ensure that the design is feasible to build. After the completion of this project, Omnium Cycles may build and test the second prototype of the Heliocycle. Note: the fabrication of the redesign was out of scope for this project.

ACKNOWLEDGMENTS

There was assistance from others in order to complete this graduate capstone project. From the Milwaukee School of Engineering, several academic faculty members provided assistance. Assistance was provided by Dr. Subha K. Kumpaty in general project advising, Dr. Nebojsa Sebastijanovic in finite element analysis, Professor Gene A. Wright in business, and Professor Gary Shimek in literary and technical expertise. A special thank you is extended to Adam Fronek for his assistance in the areas of design and fabrication advising.

TABLE OF CONTENTS

LIST OF FIGURES

LIST OF TABLES

NOMENCLATURE

Symbols

A	ampere, or amp (unit of electric current)
BTU	British Thermal Unit (unit of heat)
C	Celsius (unit of temperature)
cm	centimeter (unit of length)
F	Fahrenheit (unit of temperature)
ft	foot or feet (unit of length)
fpm	feet per minute (unit of speed)
g	gram (unit of mass)
GPa	gigapascal (unit of pressure, strength, or stress)
hp	horsepower (unit of power)
in.	inch or inches (unit of length)
ips	inches per second (unit of speed)
J	Joule (unit of work or energy)
K	Kelvin (unit of temperature)
kg	kilogram (unit of mass)
km	kilometer (unit of length)
lb_f	pound force (unit of force)
lb_m	pound mass (unit of mass)
mm	millimeter (unit of length)
MPa	megapascal (unit of pressure, strength, or stress)
mph	miles per hour (unit of speed)

N	Newton (unit of force)
psi	pounds-force per square inch (unit of pressure, strength, or stress)
rad/s	radians per second (unit of rotational speed or angular velocity)
rpm	revolutions per minute (unit of rotational speed or angular velocity)
V	volts (unit of electromotive force)
W	Watt (unit of power)

Abbreviations

AISI	American Iron and Steel Institute
AGMA	American Gear Manufacturers Association
ASME	American Society of Mechanical Engineers
BOM	bill of materials
CAD	computer-aided design
CG	center of gravity
FEA	finite element analysis
FOS	factor of safety
FT	fabrication team
HPV	human powered vehicle
HPVC	Human Powered Vehicle Challenge
Li-ion	lithium-ion
MS	Multiple Sclerosis
PPE	personal protective equipment
VRLA	valve-regulated lead-acid

GLOSSARY

Alloy[1]: "A blend of metals."

Bogie wheel[2]: "A structure underneath [the trike] to which axles (and, hence, wheels) are attached through bearings," that is, "a chassis or framework carrying wheels, attached to a vehicle, thus serving as a modular subassembly of wheels and axles."

Boom: The tubular bar that protrudes from and is fastened to the front of the vehicle. The front reaches of the boom is where the crankset is assembled to.

Brakeset[3]: "A complete brake system; levers, calipers, cables."

Cassette[4]: "The rear cog cluster on a derailleur bicycle that fits on a freehub. It consists only of cogs, with no ratcheting mechanism."

Chain: A loop of linked metal pieces that connects the crank and rear wheel that when actuated, propels the vehicle.

Cleats[5]: "The parts that are attached to the soles of cycling shoes that connect the shoes to the pedals for more efficient pedaling."

Crankset[6]: "The bicycle drivetrain assembly that converts the rider's reciprocating pedaling action to rotating motion. It consists of two cranks (or arms), one or more chainwheels (or chainrings), plus the stack bolts that connect them."

---

[1] Century Cycles, Inc., "Glossary of Cycling Terms," Century Cycles, 2016. [Online]. Available: http://centurycycles.com/glossary/glossary-of-cycling-terms-pg869.htm. [Accessed 8 November 2016].
[2] Wikimedia Foundation, Inc., "Bogie," Wikipedia, 2016. [Online]. Available: https://en.wikipedia.org/wiki/Bogie. [Accessed 8 November 2016].
[3] Century Cycles, Inc., "Glossary of Cycling Terms," Century Cycles, 2016. [Online]. Available: http://centurycycles.com/glossary/glossary-of-cycling-terms-pg869.htm. [Accessed 8 November 2016].
[4] Wikimedia Foundation, Inc., "Glossary of Cycling," Wikipedia, 2016. [Online]. Available: https://en.wikipedia.org/wiki/Glossary_of_cycling. [Accessed 8 November 2016].
[5] Century Cycles, Inc., "Glossary of Cycling Terms," Century Cycles, 2016. [Online]. Available: http://centurycycles.com/glossary/glossary-of-cycling-terms-pg869.htm. [Accessed 8 November 2016].
[6] Wikimedia Foundation, Inc., "Glossary of Cycling," Wikipedia, 2016. [Online]. Available: https://en.wikipedia.org/wiki/Glossary_of_cycling. [Accessed 8 November 2016].

Derailleur[7]: “A device used to change gears, activated by shifters.”

Drivetrain: A system comprised of the crankset, chain, derailleur(s), and pedals.

E-bike[8]: “Short for 'electric bike,' these bicycles includes battery-powered electric motors.”

Finite element method[9]: “A numerical technique for finding approximate solutions to boundary value problems for partial differential equations. It is also referred to as finite element analysis (FEA).”

Fork[10]: “Part of the frameset that holds the front [or rear] wheel. Can be equipped with a suspension on mountain bikes.”

Frame: The rigid structure that bicycle/tricycle parts attach to.

Hub motor[11]: “An electric motor that is incorporated into the hub of a wheel and drives it directly,” and may also be called “wheel hub motor, wheel motor, wheel hub drive, or in-wheel motor.”

Linear actuator[12]: “An actuator that creates motion in a straight line, in contrast to the circular motion of a conventional electric motor.”

Mirror[13]: “A reflecting surface, originally of polished metal but now usually of glass with a silvery, metallic, or amalgam backing.”

---

[7] Wikimedia Foundation, Inc., "Glossary of Cycling," Wikipedia, 2016. [Online]. Available: https://en.wikipedia.org/wiki/Glossary_of_cycling. [Accessed 8 November 2016].
[8] Century Cycles, Inc., "Glossary of Cycling Terms," Century Cycles, 2016. [Online]. Available: http://centurycycles.com/glossary/glossary-of-cycling-terms-pg869.htm. [Accessed 8 November 2016].
[9] Wikimedia Foundation, Inc., "Finite Element Method," Wikipedia, 2016. [Online]. Available: https://en.wikipedia.org/wiki/Finite_element_method. [Accessed 8 November 2016].
[10] Wikimedia Foundation, Inc., "Glossary of Cycling," Wikipedia, 2016. [Online]. Available: https://en.wikipedia.org/wiki/Glossary_of_cycling. [Accessed 8 November 2016].
[11] Wikimedia Foundation, Inc., "Wheel Hub Motor," Wikipedia, 2016. [Online]. Available: https://en.wikipedia.org/wiki/Wheel_hub_motor. [Accessed 8 November 2016].
[12] Wikimedia Foundation, Inc., "Linear Actuator," Wikipedia, 2016. [Online]. Available: https://en.wikipedia.org/wiki/Linear_actuator. [Accessed 8 November 2016].
[13] Dictionary.com, LLC, "Mirror," Dictionary.com, 2016. [Online]. Available: http://www.dictionary.com/browse/mirror. [Accessed 8 November 2016].

Pedal[14]: "A lever-like part worked by the foot to supply power in various mechanisms, as the bicycle."

Power assist system: A system comprised of electrical components. This powers the seat lift mechanism when the controller is actuated, as well as the rear-wheel motor to assist forward motion when the throttle is actuated.

Recumbent[15]: "A bicycle or tricycle where the rider is placed in a laid-back position, feet first and sitting in a seat instead of on a saddle. Usually used for ergonomics or aerodynamics."

Reflector[16]: "A body, surface, or device that reflects light, heat, sound, or the like."

Rigid[17]: "A bicycle without any suspension system."

Rim[18]: "The outermost part of the wheel. The tire mounts to the rim. On bicycles with caliper hand brakes (not disc brakes), the rim is part of the braking system."

Roller[19]: "A cylindrical body, revolving on a fixed axis, especially one to facilitate the movement of something passed over or around it."

Saddle: Another term for the seat.

---

[14] Dictionary.com, LLC, "Pedal," Dictionary.com, 2016. [Online]. Available: http://www.dictionary.com/browse/pedal. [Accessed 8 November 2016].
[15] Wikimedia Foundation, Inc., "Glossary of Cycling," Wikipedia, 2016. [Online]. Available: https://en.wikipedia.org/wiki/Glossary_of_cycling. [Accessed 8 November 2016].
[16] Dictionary.com, LLC, "Reflector," Dictionary.com, 2016. [Online]. Available: http://www.dictionary.com/browse/reflector. [Accessed 8 November 2016].
[17] Wikimedia Foundation, Inc., "Glossary of Cycling," Wikipedia, 2016. [Online]. Available: https://en.wikipedia.org/wiki/Glossary_of_cycling. [Accessed 8 November 2016].
[18] Century Cycles, Inc., "Glossary of Cycling Terms," Century Cycles, 2016. [Online]. Available: http://centurycycles.com/glossary/glossary-of-cycling-terms-pg869.htm. [Accessed 8 November 2016].
[19] Dictionary.com, LLC, "Roller," Dictionary.com, 2016. [Online]. Available: http://www.dictionary.com/browse/roller. [Accessed 8 November 2016].

Seat assist mechanism: An electro-mechanical system that raises and lowers the seat to assist the rider into and out of the vehicle. Assist may be interchanged with lift, and mechanism may be interchanged with system.

Shifter[20]: "A component used by the rider to control the gearing mechanisms and select the desired gear ratio. It is usually connected to the derailleur by a mechanical actuation cable. Electronic shifting systems also exist."

Spokes[21]: "The usually metal rods that run between the wheel hubs and rims. Spokes come in different shapes, materials, thicknesses and lengths."

Steering mechanism[22]: A system of "two handlebars (rather, two half-handlebars) each bolted to a steerer tube, usually through a bicycle-type headset and connected to a stub axle assembly (direct). A single tie rod connects the left and right axle assemblies."

Tadpole[23]: A "tricycle [that] has two front wheels and one rear wheel."

Throttle: A lever that when actuated, controls the speed of the motor.

Tiller: The specific type of handlebars used in this vehicle to turn the front wheels.

Tricycle[24]: "Like a bicycle but with three wheels. Comes in both upright and recumbent versions." Also referred to as trike.

---

[20] Wikimedia Foundation, Inc., "Glossary of Cycling," Wikipedia, 2016. [Online]. Available: https://en.wikipedia.org/wiki/Glossary_of_cycling. [Accessed 8 November 2016].
[21] Century Cycles, Inc., "Glossary of Cycling Terms," Century Cycles, 2016. [Online]. Available: http://centurycycles.com/glossary/glossary-of-cycling-terms-pg869.htm. [Accessed 8 November 2016].
[22] Wikimedia Foundation, Inc., "Tricycle," Wikipedia, 2016. [Online]. Available: https://en.wikipedia.org/wiki/Tricycle. [Accessed 8 November 2016].
[23] Wikimedia Foundation, Inc., "Tricycle - Tadpole," Wikipedia, 2016. [Online]. Available: https://en.wikipedia.org/wiki/Tricycle#Tadpole. [Accessed 8 November 2016].
[24] Wikimedia Foundation, Inc., "Glossary of Cycling," Wikipedia, 2016. [Online]. Available: https://en.wikipedia.org/wiki/Glossary_of_cycling. [Accessed 8 November 2016].

INTRODUCTION

Description of the Project

The purpose of this project was to complete the redesign and analysis of the Heliocycle, a human powered vehicle (HPV) based on a recumbent tadpole tricycle design. This HPV makes it possible for people with limited mobility to have the traditional biking experience. The trike has full pedaling capabilities (traditional experience), but also features innovations that differentiates this trike from others. In particular, the onboard electric system powers a seat assistance mechanism (a unique system that raises and lowers the seat to make mounting and dismounting the trike easier) and a power assistance system (a motor-containing rear wheel that, when actuated, spins and propels the unit forward).

Feedback received during the Heliocycle's showcases, in addition to notes made during the original prototype's build, was all recorded and several major points were addressed in the redesign. The original prototype of the Heliocycle was fabricated primarily of steel, which made it strong, sturdy, and durable, but also heavy – lighter materials were incorporated to reduce its weight. The original seat mechanism helped with mounting and dismounting the trike, but it did not have convenient or accessible features available for readjusting – handles were added to improve the ability for readjusting. The seat assistance mechanism proved useful and functional, but slow and rigid – a new mechanism was implemented to increase seat travel speed and improve comfort during operation. The electric system was reliable and had longevity, but the trike did not provide storage for backup power – additional storage was added to allow for longer rides.

A brief market analysis was conducted to determine a target audience. Originally, people battling Multiple Sclerosis (MS) were the main focus, but the analysis discovered people with similar symptoms could also benefit from this HPV. The full pedaling capability and seat and power assistances allow for people with limited mobility (or full mobility) to be able to ride. That being said, if limited mobility has prohibited people from riding, this trike can restore that ability and reintroduce exercise and a sense of independence. For these reasons, there may also be a business opportunity with this product.

Justification of the Project

The justification for this project lies within the reasons for the redesign, in addition to the reasons the initial Heliocycle was designed.

Original Vision

At first, the Heliocycle was designed for people struggling with MS. The objective of the trike was to provide a traditional bike/trike riding experience and allow for the sense of independence to be regained while doing so. A common setback of MS is the lack of independence – the disease is unfortunately very limiting in many cases, so having a tricycle that has seat and power assistance can give someone independence again. However, the audience has since been expanded to people with limited mobility, but the same conclusions still apply. Furthermore, this vehicle can be used as a tool of exercise. With full pedaling capabilities, this trike may provide good physical activity. More benefits of this trike come with the ability to do group activities and to enjoy the outdoors while doing so. Because this trike can be used by someone with limited mobility, group rides can be easier to do, too.

Future Sights

Important feedback was received after the Heliocycle reached several audiences. Getting input from different people with various forms of mobility-limiting inhibitors led to ideating several design improvements. Among the many suggestions, the redesign featured attempts to make the trike lighter (overall weight), faster and more comfortable (seat assistance mechanism), and more versatile (store more power source). Ideally, the redesign would also reduce costs so that the trike can be more affordable for more people. The feedback was ample and eager, which suggests there is definitely a need for this product.

Furthermore, it would be ideal to expand the target audience to be able to reach more people. The original audience consisted of people specifically with MS, but expanding to people with limited mobility may result in a larger impact. There have been studies and investigations that looked into the effect exercise has on MS (decreasing its symptoms), so that is another facet of this project that was explored. Any evidence that supports this theory (the idea that exercise can improve the well-being and health of low mobility individuals) may be used for additional justification for this project.

BACKGROUND RESEARCH

There was background research conducted to find existing technology and relevant literature. This information was used for insight into how this project could improve upon what already exists, and a potential market was identified.

Existing or Similar Technology

Recumbent Design

The recumbent tricycle design is ideal because it combines the comfort of the recumbent riding position with the stability of a tricycle. Comfort is very important on long rides, where cyclists may be in the same position for extended periods of time. Because limited mobility may make it difficult to balance a typical bicycle, having a stable trike is important.

The recumbent design, as seen in Figure 1, is an excellent solution for long rides because of the reduced stress on the lower back. However, the one issue with this design is that it still requires the rider to balance the bicycle, which could be difficult for someone with limited mobility. To overcome this, a recumbent tricycle was used to increase the stability of the HPV while keeping the comfort of a recumbent bicycle.

Figure 1: Example of a Recumbent Bicycle [1].

A tricycle with two wheels in the front and one in the back is known as a tadpole tricycle, as seen in Figure 2. The main benefit of the tadpole design is that the rider can be seated lower to the ground, resulting in a lower center of gravity (CG). By being lower to the ground, the tricycle is more stable around turns and is less affected by wind resistance.

Figure 2: Example of a Recumbent Tricycle [2].

One problem with the tadpole design is the potential for the tricycle to tip forward during immediate braking if the front brakes are applied suddenly. This can occur if the tricycle design has too much weight in the front, causing the CG to be forward of the tipping axis, as seen in Figure 3. To overcome this, more weight would need to be distributed toward the rear of the tricycle. This ensures the CG remains behind the tipping axis for maximum stability [3]. The seat being lower may also make it more difficult to get into and out of.

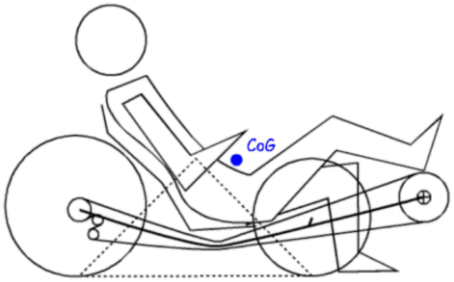

Figure 3: Center of Gravity of a Tadpole Tricycle [3].

The second type of typical recumbent tricycle, known as a delta tricycle, has two wheels in the back and one in the front. The delta tricycle usually positions the rider slightly higher than a tadpole design. Because the weight of the rider and wheels are toward the back, it does not have the problem of tipping forward when braking suddenly. However, because the CG is typically behind the tipping axis, as seen in Figure 4, the delta tricycle is more likely to tip backwards when traveling up a hill [3].

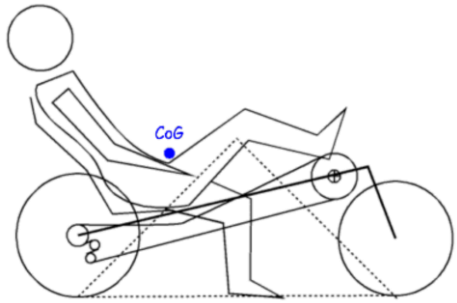

Figure 4: Center of Gravity of a Delta Tricycle [3].

Power Assistance

Power assistance was implemented on the HPV in order to assist the target audience inhibited by various forms of limited mobility. The power assistance is able to help the rider when fatigue sets in too, or fully power the vehicle if mobility restrictions prohibit the ability to pedal independently. This feature is called power assistance and not pedaling assistance because one wheel of the trike (the rear wheel) contains a motor. When activated, the motor propels the trike forward without the pedals moving or needing to be pedaled. If the pedals needed to be (or were) moved when the power assistance was actuated, a more correct term could be pedal assistance.

The three main types of power assistance used on bicycles are: electric, pneumatic, and hydraulic. HPVs powered by hydraulics use either a hydraulic cylinder or motor to power the HPV, as seen in Figure 5. An accumulator can be implemented in the

system to store energy generated from downhill riding. This energy would then be discharged while the rider is traveling uphill. However, the amount of energy discharged by the accumulator does not make up for its weight of typically 15 lb_m [4]. Along with the increased weight from the hydraulic components, another challenge when designing with hydraulics is that they may have a poor low-speed efficiency.

Figure 5: Example of a Hydraulically Powered Recumbent Tricycle [4].

HPVs powered with pneumatics have similar components as the hydraulic HPVs. The pneumatically powered vehicle components consist of reservoirs of pressurized air that power a pneumatic cylinder, which powers the vehicle, as seen in Figure 6. Accumulators can also be used in pneumatically powered vehicles to store the generated energy. Pneumatic systems are generally more environmentally friendly, weigh less, cost less, and have less pipe-flow losses than hydraulically powered vehicles [4].

Figure 6: Example of a Pneumatically Powered Bicycle [4].

The most common type of power assistance for bicycles is electric. Electronically powered vehicles are driven by an electric motor that is powered by a battery, as seen in Figure 7. Similar to the accumulator in the hydraulic and pneumatic systems, excess energy can be captured by regenerative braking in electric systems. There are many electric bicycle kits on the market that contain an electric motor, controller, battery, and all other integral components to convert any existing bicycle into an electric bicycle (e-bike). These kits can be expensive because of the cost of the battery.

Figure 7: Example of an Electrically Powered Bicycle [5].

The battery used to power the electric motor must have deep-cycling capability since the battery is usually discharged to around ten to twenty percent state of charge

(percentage of full charge) [5]. The battery also requires a high specific energy in order to achieve an adequate range [5]. The two main types of batteries that meet these requirements are valve-regulated lead-acid (VRLA) and lithium-ion (Li-ion). A comparison of VRLA and Li-ion batteries can be seen in Table 1.

The batteries used for the comparison in Table 1 were sized to support a 60 km range and a 350 W motor [5]. From the comparison, the Li-ion battery was able to obtain the same range as the VRLA battery, while weighing 18 kg less than the VRLA battery, but costing more.

Table 1: Comparison of Battery Types [5].

Comparison of battery types (with assumptions)

Results	VRLA	Li-ion [30]
Cost ($)	75	424
Mass (kg)	26	8
Lifetime (years)	3	9
Volume (L)	10	5
Max theoretical power (kW)	6.2	2.9
Recharging safety	High	Low
Temperature effects	Moderate	High

Assumptions	VRLA[a]	Li-ion
Specific energy ($Wh\,kg^{-1}$)	35	110
Energy density ($Wh\,L^{-1}$)	86	170
Power density ($W\,kg^{-1}$)	240	350
Cost ($\$\,kWh^{-1}$)	83	505[b]
Cycle life	300	800

[a] Data for VRLA come from Chinese battery measurements and product brochures.

[b] Zhengke Li-ion battery e-bike (anonymous source).

Braking

The brakes on the HPV have two main purposes: to stop the vehicle gradually or suddenly, and to control the vehicle's speed on long downward hills [6]. The HPV may use bicycle brakes to achieve these main purposes. There are multiple options for bicycle

brakes on the market: coaster, rim, disc, and hydraulic disc. Each of these options feature both advantages and disadvantages, which were discovered in the research.

Coaster brakes consist of a rear hub that allows the rear wheel to turn without the pedals moving, and they stop the bicycle when the pedals and crank are turned backwards. Coaster brakes are grease-lubricated and struggle handling the high temperatures created by downhill runs. The grease will begin to smoke at a seven hundred fifty foot drop at a nine percent grade [6]. Bicycles that contain only coaster brakes require fifty percent more stopping distance on average [6].

Rim brakes consist of two rubber brake pads that apply friction to the metal rim of the wheel to stop the bicycle, as seen in Figure 8. The high amount of drag force being applied to the metal rims from the rubber brake pads causes a large amount of wear on the rim and brake pads over time. The weather can also affect the performance of the rim brakes as mud, dirt, and water is picked up from the ground by the metal rim and gets under the brake pads when applied. This may cause a longer stopping distance or failure for the brakes to engage at all.

Figure 8: Example of a Rim Brake [7].

Disc brakes consist of a caliper that clamps down on a metal disc that is mounted to the hub of the wheel to stop the bicycle, as seen in Figure 9. Disc brakes are not affected by the weather since the metal disc is mounted to the hub of the wheel and does not come in contact with the ground. The addition of the frictional surface area (the metal disc) increases the weight of the braking system. By using the metal disc as the frictional surface area, disc brakes do not cause any wear on the metal rim of the wheel. The metal disc has a smaller amount of surface area exposed to the air, causing disc brakes to be designed to withstand higher temperatures than rim brakes. Disc brakes require larger brake-shoe forces with little brake-shoe movement, which requires the brake-shoe materials to be rigid and capable of withstanding higher temperatures. These material properties result in materials with lower coefficients of friction, which in turn increases the amount of required brake-shoe forces to stop the bicycle [6].

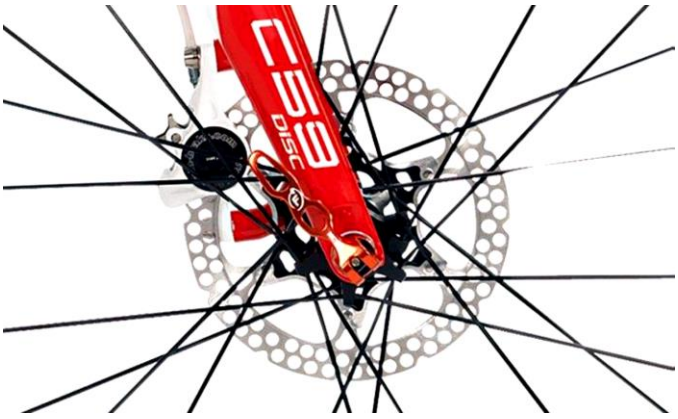

Figure 9: Example of a Disc Brake [8].

Hydraulic disc brakes operate in the same manner as the mechanical disc brakes; however, instead of using brake cables, hydraulic disc brakes use hydraulic fluid to engage the brakes. Hydraulic disc brakes provide a large amount of force within a short movement of the brake pads by the use of large-area brake pistons [6]. If failure occurs in the hydraulic brakes, they are not easily able to be repaired in the field.

Heliocycle

The present trike effectively overcomes the issues directly related to getting in and out of the HPV. The seat lift system allows the operator to be safely lowered into the vehicle and raised back out. The range of motion needed to safely use the seat lift system was found to be significantly less than that of current cycling vehicles. Another advantage of this trike is that the seat lift system may be powered by the power assist system. A full-body range of motion is not necessary in order to use the seat lift system, thus making it usable for low-mobility individuals.

Figure 10 shows the existing configuration (original design) for this trike. Main features include: the frame (1), the seat (2), the seat lift/adjusting mechanism (3), the boom (4), the pedals and crank (5), the steering mechanism (6), the brakes (7), the steering tiller system (8), the hand brakes (9), the hand throttle (10), the rear-view mirrors (11), the power assist encasement (12), the hub motor (13), and the safety flag (14). Other features are possible, and not all features are required for the trike to function. A bottle cage/holder, lighted rear turn signals and emergency flashers, and an extra storage compartment cannot be seen in Figure 10, which are optional features as well. Some uncommon terms may be found in the Glossary.

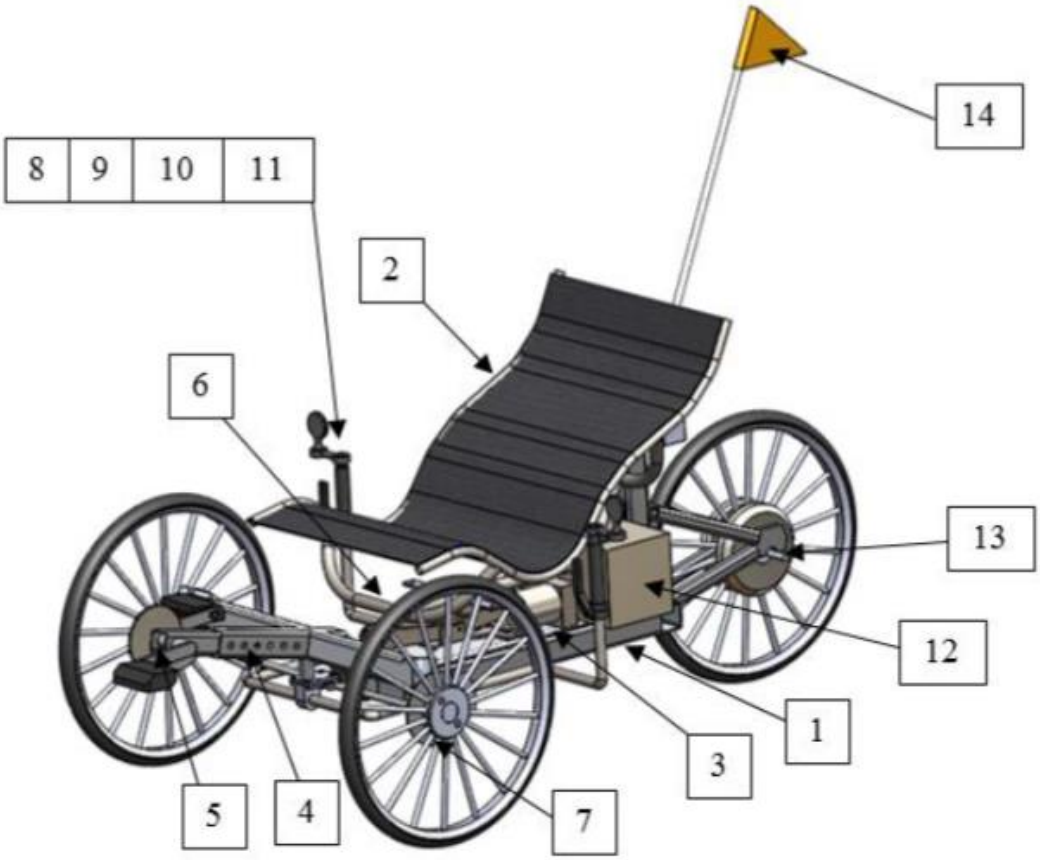

Figure 10: An Isometric View of the Heliocycle [9].

Figure 11 (left) shows a side view of the initial Heliocycle CAD model with the seat lowered. This position is recommended for use when the trike is being ridden. Figure 11 (right) shows a side view of the initial Heliocycle CAD model with the seat raised. This position allows for the rider to get into and out of the trike using less full-body range of motion.

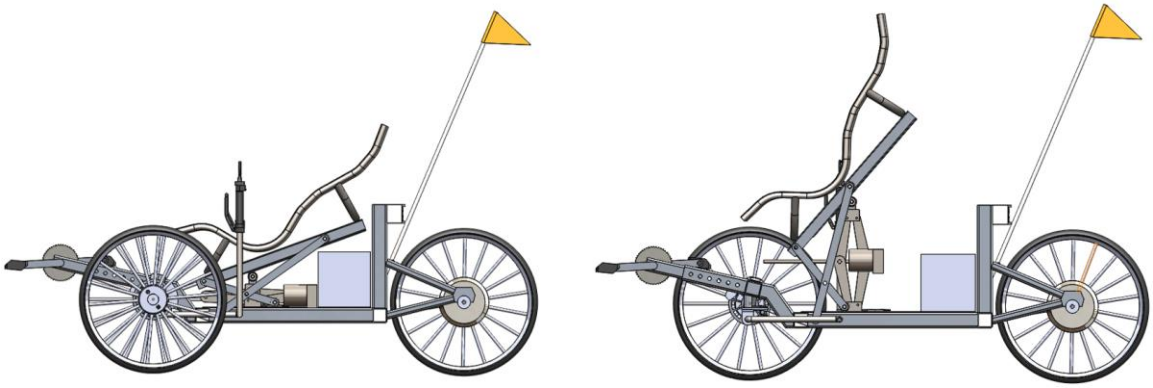

Figure 11: Initial Heliocycle in Lowered Position (left) and in Raised Position (right) [9].

The existing seat lift system of the Heliocycle is electro-mechanical, and it is connected to the power assistance system. To activate the seat lift system, the operator presses an up (or down) button on the seat lift controller, which would raise (or lower) the seat. The controller in the initial design is a hard-wired remote connected to the power assistance system. The seat lift system is fully capable of supporting the rider from the minimum (lowered, Figure 11, left) to the maximum (raised, Figure 11, right) position.

In the initial design, the lifting mechanism is a combination of rollers, linkage arms, and a carjack device. From the lowered position, as the device is powered, it pushes up on the seat base. The linkage system then extends upward and outward, thus assisting the rider up and out of the trike. Conversely, from the raised position, as the device is powered, it slowly and in a controlled manner collapses downward, thus lowering the seat (and rider is mounted in the seat).

Prominent feedback from this design was factored into and focused on during this redesign. First, the structure of the trike is very durable, but it is too heavy (especially for one person to lift; it should be lifted by at least two people as the original prototype weighs approximately 136 lb_m). It was also suggested that handles be added to the seat so that there is something convenient to hold onto while mounting/dismounting the trike.

Also, these handles could then be used to readjust the rider's position if needed while in the trike. Next, the seat lift mechanism is extremely useful and robust, but its speed could be increased. Last, the range of the power assistance is a function of several variables: amount used, rider size, terrain and weather. It was found the range of the battery may decrease with more battery use, the larger the rider, the steeper/longer the inclines, and the more inclement the weather. This being said, it was suggested that there be additional onboard storage for a secondary backup battery, if desired (for longer distance rides, or just in case of an emergency).

Potential Market

Market Description

The bicycle market in the United States is a huge market. With revenues exceeding $848 million and growing 0.5% in the past five years, there is definitely a business opportunity available in this market [10]. Continuing, the revenue outlook is expected to grow in excess of $886 million by the year 2022 [10]. The bicycle and tricycle market are oftentimes linked, since their natures are so similar. Therefore, it can be anticipated that as the bike market excels, the trike market will, too. Some inventors and entrepreneurs have caught wind of this trend and have capitalized on it. There are several trike companies, such as TerraTrike and Catrike. These two companies are making tricycles for different purposes (e.g., leisure, speed, etc.), so it may only be a matter of time when they expand their engineering to accommodate for special needs or disabilities.

Customer Description

The targeted customer for this product is someone who is restricted by some form(s) of limited mobility or old age. Some mobility-limiting symptoms may include fatigue, numbness or tingling, weakness, dizziness and vertigo, pain, walking difficulties, spasticity, vision problems, and cognitive changes, to name a few. Users who may experience any/all of these symptoms, or any similar, could be eligible customers. Safety, stability, and usability are all primary focuses in the original design and redesign of this trike. Nevertheless, fully-abled bodies may still operate this HPV. Limited mobility need not be a requirement to purchase or operate a Heliocycle trike.

What They Want

There are people who were once able to ride a bicycle or tricycle and can no longer do so safely, because of physical and/or mental limitations. There are also people who were never able to ride a bike or trike who may want to experience that style of exercise, recreation, or competition. Some people who have and no longer can, or those who never could and want to, aspire to get on the path and trike safely. The trike also features many benefits, as listed in the Product Specifications section.

How They Buy

According to current plans, customers will eventually purchase and obtain trikes through a few different avenues. One route to take would be going online to Omnium Cycle's website and purchase directly from there. Another option to possibly get this trike would be through the customer's insurance company. Some insurance companies have begun to prescribe physical exercise and physical therapy as a means to treat limited

mobility diseases. Through insurance companies, this trike may be purchased for those who qualify.

Best Ways to Communicate with Customers

There are several ways to communicate with customers. Omnium Cycles' website and social media (Facebook, Twitter, etc.) are all mediums to relay information to the user/customer, present or potential. This is the digital way to communicate, but word-of-mouth is another valuable method. Additionally, the trike appears in and makes trips during the Wisconsin Bike MS: Best Dam Bike Tour, which is a fantastic way for many people to see it and to provide feedback. Other forms of communication other than those already listed are, but are not limited to, emails, phone calls, trade shows, conventions, bike ride fundraisers, and paid advertising.

Literature Review

Patents and Prior Art

Research was conducted for prior art in order to avoid infringing on any patents while designing this HPV. Several of the patents found in the research are summarized below, but this list may not be fully exhaustive with respect to all relevant literature. The last patent is a summarization of the patent pending for the Heliocycle.

Patent number 8,544,947 [11] is titled, "Bicycle Fitting Apparatus and Method," and it refers to an apparatus used to fit a saddle on a bicycle. The apparatus allows the saddle to be adjusted vertically and laterally. In addition, the apparatus enables the seat to be tilted and includes a clamp to secure the saddle to the desired tilted position. Patent number 3,598,195 [12] is titled, "Electric Tricycle," and it refers to a tricycle that is pedal-operated as well as electrically operated by a battery-powered drive motor. The

tricycle can be powered by either source individually or in combination with each other. Both power sources provide power to the rear axle.

Another patent, numbered 4,887,829 [13] is titled, “Rear Wheel Suspension System for a Tricycle Vehicle,” and it details a three-wheeled vehicle with one front wheel for steering and two rear wheels. The rear wheels are connected by a suspension consisting of swing arms, which are connected to rocking arms via roll joints. This suspension allows the vehicle rider to lean the vehicle while turning. Lastly, there was a provisional patent filed and received for the Heliocycle, numbered 62/392,107 [9], and titled, “Vehicle with Seat Lift System.” It describes how the invention relates to cycling vehicles, but more specifically to the seat lifting system of a cycling vehicle.

Codes and Standards

Several codes and standards were followed throughout this project, and brief descriptions of these can be found in Appendix A.

Bicycles and FEA

Finite element analysis is “a numerical technique for finding approximate solutions to boundary value problems for partial differential equations” [14]. FEA has been used on a multitude of different applications. No matter the application, though, a typical purpose of FEA is to use “variational methods from the calculus of variations to approximate a solution by minimizing an associated error function” [14]. Using FEA in the particular application of bikes and trikes can prove useful since frames or components can be analyzed on a computer before any prototypes are made and tested. This can result in less cost for a company (or other entity). Also, early and frequent FEA on a design can

reveal design weaknesses or flaws, which can reduce recovery work and fixes later in a product's design life.

FEA can further be useful in the bike and trike world to test various configurations and frame structures. For instance, FEA can be a tool used on testing the strength or delta or tadpole configurations for trikes [15]. In addition to using FEA to analyze the trike frame, the wheel base, track width, weight distribution, tires and rims, braking system, suspension system, steering system, and transmission system may all be analyzed using various finite element methods [15]. Completing FEA on any of these categories or systems can prove a design is functional/safe or dysfunctional/unsafe, where either or both can be useful knowledge.

Bicycles and MS/Paraplegia

There have been studies suggesting exercise can combat the symptoms of MS and other related paraplegia [16]. This area of research is still ongoing, but it directly relates to this project. Since one of the main goals of the Heliocycle is to be a tool for exercise for people with MS and/or limited mobility, studies that find when exercise can help reduce the struggles of limited mobility are all useful in establishing a larger market. Not only are there studies researching how exercise helps improve the body, some of the same studies are investigating how to ease the mounting and dismounting of the trike. Any findings and feedback from testers can be useful information.

Power assistance, pedaling, braking, and safety are all major concerns for most riders who battle MS or paraplegia. That being said, these are major design considerations, and when possible, backups are designed into the trike in case the primary function for the rider is inoperable. Thus, these are some areas that are looked into

carefully in these studies [16]. Having orthopedic problems (not necessarily diseases or permanent disabilities) or old age (and limited mobility) are the subject for more studies as well [17]. There are a wide variety of inhibiting factors that can limit a rider's body and range of motion, so there are studies being conducted to investigate the benefits of exercise to help combat these disabling symptoms.

Aside from studies investigating ways exercise can improve the health and well-being of riders, there are kits being made that can transform a wheelchair into an electric tricycle [18]. With a reported 15% of the world's population having a disability, a kit to help mobilize people who primarily travel by wheelchair can become very helpful and useful to more than 1 in 10 people [18]. Whether it is getting people with a disability into an electric-assisted trike, or providing them with a kit to connect to their wheelchair, there are ways being explored to help mobilize people.

Mechanics of Tricycles

The functionality of trikes from one model to the next is extremely similar, but each brand carries its own personal touch. Tadpole and delta recumbent trikes operate very similarly, but a few key differences can really tell the two apart. A tadpole trike has two wheels in the front and one wheel in the back, whereas a delta trike has one wheel in the front and two wheels in the back. In addition to that fundamental difference, the position of the pedals is very important for each configuration. Since the delta trikes have one wheel in the front, the rider's legs must split in order to reach the pedals (typically), whereas the rider's legs strut through and between the two front wheels of a tadpole trike.

Also, if a trike is equipped with motor-containing wheels, the configuration may become more crucial. Having one (or two) motorized wheels in the front (or back) can

change how the trike responds and performs [19]. In summary, the trike configuration and electrical assistance layout are both connected and important to consider.

Another important feature to consider is the steering mechanism. On many trikes, the Ackermann steering geometry is used, but other methods could be implemented [15]. In conjunction with the steering mechanism is the steering system – a steering wheel, small handles, large tillers, are just some of the options that can be incorporated in the trike design.

The overall design of the trike may also be a major contributing factor when designing a trike. Since the Heliocycle has purposefully neglected a windshield, optimizing aerodynamics during the designing was not a major design constraint. Nevertheless, trikes that have body shape enclosures may focus lots of design and analysis time and effort to get the shell aerodynamically optimized [20].

Many trike mechanics must be considered during the design process, but the major design feats are accomplished when the frame configuration and steering mechanism system are designed and established.

PRODUCT SPECIFICATIONS

Design Objectives

The HPV redesign has met the following objectives:

- Adjustability
    - Boom is adjustable to accommodate riders of different heights.
    - Seat is able to raise/lower to assist the rider in/out of the seat.
- Aesthetics
    - HPV maintains the visual appearance of a traditional tadpole trike.
    - Color scheme resembles a modern, clean, and stylish appeal.
- Electrical equipment
    - Battery has the capability to be recharged from standard wall outlets.
    - Onboard electronics are enclosed to prevent electrical shock hazards.
- Exercise
    - Trike can be used as tool in rehabilitation from mobility-limiting diseases.
    - Enjoyment of the outdoors can be regained while incorporating exercise.
- Independence
    - Power assistance eliminates needing help from someone else.
    - Seat assistance mechanism and power assistance system enables freedoms.
- Safety
    - HPV has turn signals (blinkers) and reflectors.
    - Engineering design/analysis has ensured quality, durability, and safety.

The main objective of this HPV was to provide people with limited mobility a way to enjoy the biking experience without feeling held back by the effects of the disease. In order to successfully do this, the rider will need to feel like the HPV is no different than any other tricycle. Therefore, the first design objective was that the aesthetics of the HPV must maintain the visual appearance of a traditional tadpole tricycle. This means there are two front wheels, one located on each side of the rider, and one wheel centered behind the rider. The pedal setup was designed similar to a recumbent bicycle, located out in front of the rider, with the chain running under the trike frame to the back wheel. The tricycle was also designed with the ability to be completely human powered until the rider chooses to use the electric power assist.

The electronics on the HPV involved design objectives as well. The battery that powers the electric assist was chosen so that it could be charged from a standard wall outlet (typically 120V). This allows the rider to have the ability to recharge the batteries with a common power source throughout the United States. Secondly, all electronics involving the battery and electric assist are to be enclosed. This will keep the electronics safe from outdoor elements that the tricycle could be exposed to during use. The enclosures act as a form of safety, by preventing the chance of someone hurting themselves if the electronics are tampered with.

The HPV also incorporated other design choices to improve the safety of the rider. The first objective was to include safety reflectors and turn signals on the tricycle. By having turn signals, the rider could keep both hands on the handles during a turning operation instead of having to remove a hand to perform hand signals. This may prove very advantageous for people with limited mobility.

How easily and comfortably the HPV can be operated is especially important to riders on any distance rides, but long distances in particular. With this is mind, design objectives for the adjustability needed to be met. First, the boom was designed to be adjustable (forward and backward) in order to change the distance from the seat to the pedals. This allows the trike to be used in a comfortable position regardless of the rider's height (and leg length). The second design objective with the seat was a lifting mechanism to help lift the rider down into the trike when mounting, and to help lift the rider up out of the trike when dismounting. This was an important feature because some riders with limited mobility may have a hard time getting into and out of the seat because of how low the tricycle is to the ground. The redesign also features a small shock absorber to improve the comfort of riding.

Design Constraints

The HPV redesign has met the following constraints:

- Accessories
    - There is 1 bottle holder mounted to the HPV.
    - There is 1 basket mounted on the HPV to hold personal essentials.
- Braking
    - The vehicle will demonstrate that it can come to a complete stop from a speed of 18 mph in a distance of 23 ft (based on ASME HPVC rules).
- Dimensions
    - The maximum width of the HPV is less than 4 ft (the minimum width of a bicycle lane is 5 ft against a curb or adjacent to a parking lane).

- Maneuverability
    - The vehicle will demonstrate that it can turn within a 13 ft radius (based on ASME HPVC rules).
- Power assist
    - The motor will be able to attain a top speed of at least 18 mph.
    - In a single charge, the battery will be able to maintain a speed of 18 mph for 50 miles carrying a 300 lb_m rider (the recommended maximum rider size/load).
- Safety
    - There is 1 rear-view mirror mounted on the HPV.
    - There is 1 safety flag mounted on the back of the HPV.
    - All surfaces of the vehicle will be free from sharp edges, protrusions, and other hazards.
- Weight
    - Vehicle has not exceeded 100 lb_m (vehicle only; without user).

METHODS

To complete this project, a five-stage formal design process was followed, as shown in Figure 12.

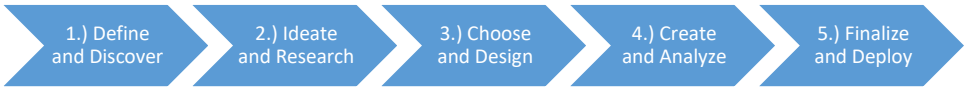

Figure 12: A Pictorial of the Five-Stage Design Process to Complete this Project.

During the Define and Discover stage, the engineer and fabrication team contacts met and discussed the needs of this project, which were identified and outlined. This project was focused on the redesign and analysis of the Heliocycle tricycle. Key changes from the existing prototype included lighter materials, handles on the seat, a new seat assistance mechanism, and additional storage for the power system. These changes in turn made the trike lighter, easier to adjust in, quicker to get into and out of, more comfortable while riding, and able to go longer distances.

In the Ideate and Research stage, the project was investigated and researched. Possible redesigns were generated, a project plan and schedule was defined, and milestones were listed. It was also determined in this stage that fabrication was out of scope for this project; therefore, funding was not necessary. If fabrication was in scope, sources for funding would have been explored in this stage.

After all of the research was completed, the best design was determined in the Choose and Design stage. In this stage, sketches, computer-aided design (CAD) models, and an outline were created to show how the design would look and be implemented. Once these were developed, they were used as the design plan.

Once the design plan was formulated, scrupulous engineering ensued in the Create and Analyze stage. This was comprised of the analyses of materials selection, mechanics of materials, and finite element analysis (FEA). More specifically, a factor of safety for the maximum load was determined after using the Pugsley Method, gear analyses were completed using AGMA standards (following guidelines and formulas presented in the Tenth Edition of *Shigley's Mechanical Engineering Design* [21] textbook), and FEA was completed on the frame to ensure its integrity under the maximum load. The engineering analysis was used to validate the design and potentially reveal any design flaws. If fabrication was in scope, the necessary resources would be gathered to build, test, and evaluate the product, and then any essential modifications would be made.

In the last stage, all project documentation was formalized and finalized, and then delivered to the advisory committee in the Finalize and Deploy stage. This would also the stage where a product would be delivered if fabricated.

While implementing this five-stage design process, a schedule was created and followed (as shown in Table 2 and Table 3), which included dates, tasks, and milestones.

Table 2: Scheduled Tasks and Milestones for the Design Phase (GE-797).

Week	Scheduled Start Date	Task	Milestone	Scheduled End Date
01 (01)	09/06/16	Organized feedback from initial prototype exposure	Had a list of ideas to improve existing design	09/11/16
02 (02)	09/12/16	Determined which changes will/not be made	Had a list of changes and non-changes	09/18/16
03 (03)	09/19/16	Ideated ways changes can be implemented	Had a compilation of ideated solutions	09/25/16
04 (04)	09/26/16	Determined how the changes will be made	Had a list of changes and their implementation	10/02/16
05 (05)	10/03/16	Met with the FT for 1st time to discuss changes	Had 1st meeting with and feedback from FT	10/09/16
06 (06)	10/10/16	Began the redesign	Had an initial design	10/16/16
		Began the progress report	Had a rough draft	
07 (07)	10/17/16	Continued the design and report	Had an improved design and draft	10/23/16
08 (08)	10/24/16	Met with FT for 2nd time to review CAD	Had 2nd meeting with and feedback from FT	10/30/16
09 (09)	10/31/16	Updated CAD to reflect advice from FT and continued progress report	Had an improved design and draft	11/06/16
10 (10)	11/07/16	Made final changes to CAD redesign	Had final CAD model	11/13/16
		Completed and submitted draft to committee	Had draft completed and submitted	
11 (11)	11/14/16	Presented the redesign and parts of the draft	Informed committee of progress in project	11/19/16

Table 3: Scheduled Tasks and Milestones for the Analysis Phase (GE-798).

Week	Scheduled Start Date	Task	Milestone	Scheduled End Date
01 (12)	11/28/16	Organized feedback from committee	Had a list of advice from committee to improve CAD and report	12/04/16
02 (13)	12/05/16	Chose what suggestions will/not be implemented	Had list of CAD and report changes	12/11/16
03 (14)	12/12/16	Met with FT for 3rd time to discuss changes suggested by committee	Had 3rd meeting with and feedback from FT	12/18/16
04 (15)	12/19/16	Updated CAD and report	Had updated CAD (final at this point) and report	01/08/17
05 (16)	01/09/17	Began the engineering analysis of redesign	Had initial FEA of frame completed	01/15/17
06 (17)	01/16/17	Continued the analysis	Had refined FEA of frame completed	01/22/17
07 (18)	01/23/17	Continued the analysis	Had gear stress analysis completed	01/29/17
08 (19)	01/30/17	Chose a linear actuator and continued the analysis	Had all off-the-shelf parts selected	02/05/17
09 (20)	02/06/17	Met with FT for 4th time to review design	Had 4th meeting with and feedback from FT	02/12/17
10 (21)	02/13/17	Finalized any analysis and CAD	Had final CAD model and analysis completed	02/19/17
		Completed and submitted report to committee	Had report completed and submitted	
11 (22)	02/20/17	Presented the final CAD, analysis, and report	Informed committee of project completion	02/25/17
		Revised CAD and report as advised by committee	Had final CAD, analysis and report completed and submitted	

RESULTS AND DISCUSSION

The redesign of the Heliocycle can be summarized into three main categories: the organization of feedback and ideating of solutions, the development of a CAD model, and the completion of the analyses. The Design Phase of the project (see Table 2) consisted of the first three stages of the formal design process described in the Methods, as well as the first part of the fourth stage. The second part of the fourth stage and the entire fifth stage were completed in the Analysis Phase (see Table 3).

Idea Generation

Of all the feedback that was received from the initial prototype of the Heliocycle, there are five suggestions that were implemented into the redesign. Those are: make the trike lighter, incorporate handles on the seat, increase the speed of the seat lift mechanism, improve the comfortability of the trike while riding, and provide additional storage for an additional battery if two are desired.

One way to reduce the weight of the trike would be to exchange existing heavy materials for lighter materials, that is, less dense or thinner-walled materials. The existing trike is made primarily from mild steel, so the redesign features aluminum wherever possible. A backup solution was to use a different steel (perhaps chromoly), or carbon fiber. The setback with carbon fiber, though, is its manufacturability and cost – the FT would have more difficulties building with it, and it would be more expensive. Changing materials can also lead to different riding comfortability, as different materials absorb impacts differently.

More weight reduction came from the different seat lift mechanism – discussion on this will follow discussion on the seat lift mechanism used for this redesign.

Unfortunately, some weight was added after the handles were implemented to accommodate the feedback that was received. The physical addition of parts to the trike inherently add weight. When added features were suggested and then designed into the trike, their form, function, and weight were all considered.

Adding handles mounted to the seat was common feedback. Many people who tested the Heliocycle (who also have limited mobility) use a walker or wheelchair to get around. Before the rider is positioned in front of the trike, the trike needs to be in a locked, parked position to prevent rolling while the rider mounts the seat. Second, the seat lift mechanism needs to be raised. Third, the pedals that are fastened to the crank of the Heliocycle are collapsible, so they can be folded down to make it easier for the rider to mount the seat (this step is optional). Once these operations are completed, the rider can stand in front of the trike, sit back into the seat, and lower the seat lift mechanism into the down position.

The feedback suggested that handles should be placed on the seat for riders to hold onto while mounting the seat and lowering into the trike. Then, once in the lowered position, the handles can be used for readjustments if necessary. The design of the handles was simple but strategic. It was important to have the handles mounted to the seat lift mechanism itself, not the frame. The handles could not be resident to the stationary frame, since the handles need to travel with the seat as the seat lift mechanism is actuated. Furthermore, the handles were designed to be comfortable, light, and skid-resistant.

There are numerous ways to increase the speed of the seat lift mechanism. The initial design incorporates a carjack device (see Figure 13 for carjack similar to one in initial design) and rollers with linkage arms. For a right side view of the original

Heliocycle CAD in its lowered and raised positions, refer to Figure 14 and Figure 15, respectively.

Figure 13: Example of a Carjack Similar to the One Used in Initial Heliocycle [22].

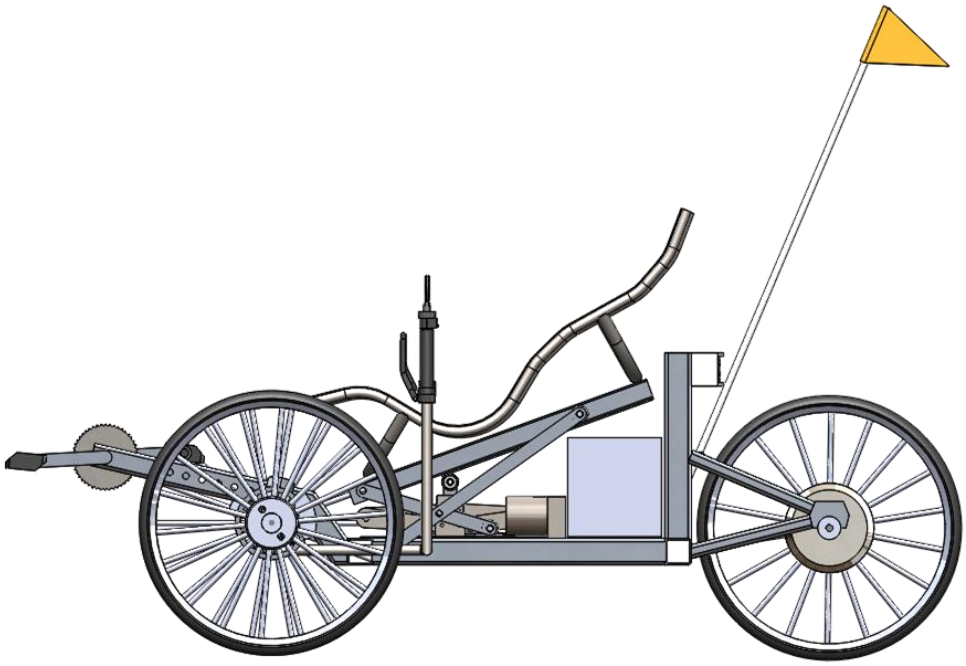

Figure 14: Side View of Original Heliocycle CAD in Lowered Position [9].

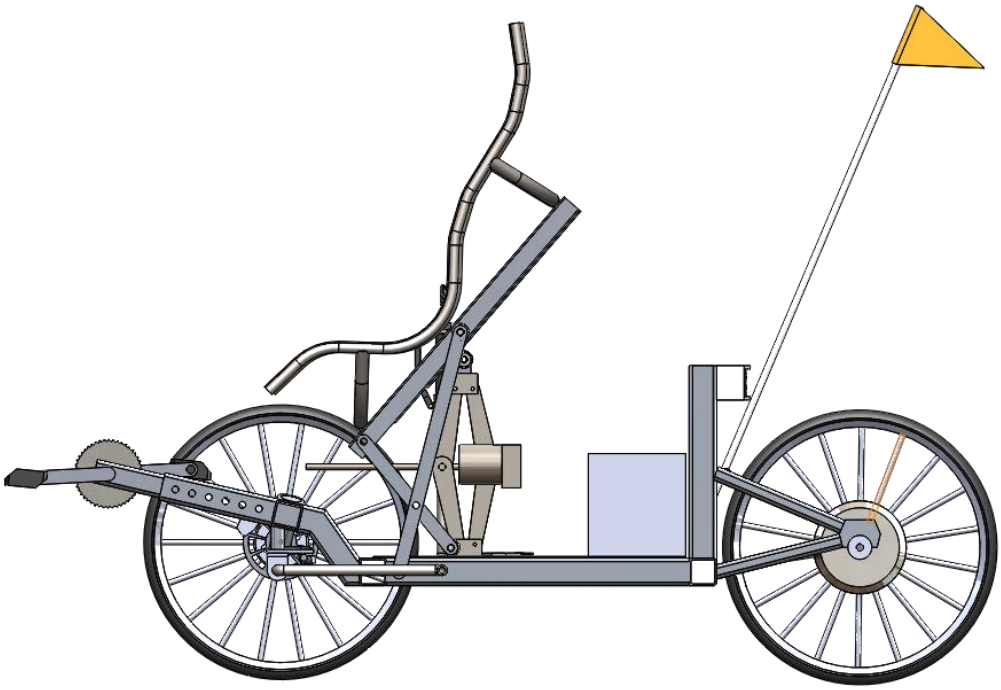

Figure 15: Side View of Original Heliocycle CAD in Raised Position [9].

A simple fix would be to replace the existing carjack with a superior jacking device, one that can support the load requirements, is lighter, and can operate at a faster speed (e.g., possibly a screw jack, as seen in Figure 16).

Figure 16: Example of a Screw Jack [23].

However, in an effort to reduce the overall weight of the trike, a new, different seat assistance mechanism was explored. The initial design has a baseplate on the bottom

of the frame to act as the base for the carjack device, but this adds weight; therefore, the carjack and baseplate were removed from the design. From here, several new seat lift mechanisms ideas were ideated, but the list was narrowed to the following concepts.

The first concept retained the linkage and roller system, but added a rotary actuator (as seen in Figure 17) as the driving input for the seat lift mechanism. Near the front of the trike, the longer linkage arms are pinned. These pins would be raised to just immediately above the frame, and these ends of the longer linkage arms would receive a spur gear (fastened or welded to the pin axes). These spur gears would then be coupled with the rotary actuators. It was not determined if one or two rotary actuators would be needed (one for the whole system or two – one for each side). Therefore, once the rotary actuators were activated, they would force the linkage system to raise or lower.

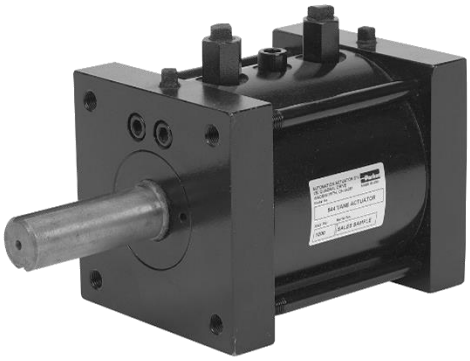

Figure 17: Example of a Rotary Actuator [24].

A quick torque calculation (force multiplied by distance equals torque moment) determined an approximate size for the rotary actuator. Rotary actuators and servo motors were researched, but very few were found that could deliver enough torque and fit within the space allotted for one. The devices that may have been feasible produced an output shaft speed of high revolutions per minute (speeds too fast for this application) and torques that would not support the projected maximum loads. Therefore, this application

would probably require a gearbox to reduce the shaft speed and increase the torque. The inclusion of one or two rotary actuators or servo motors, plus gearboxes, would not be cost or weight effective.

The next potential solution incorporated ball screw actuators and the existing linkage system (as seen in Figure 18). Two ball screw actuators would replace the two lower rollers (the rollers attached to the end of the shorter linkage arms). The load-bearing carriers would specifically replace the rollers, so these carriers would need to have a pin of some sort to be able to revolve about an axis as the seat lift mechanism is actuated and the linkage system raises or lowers. Research discovered a wide range of ball screw actuators, varying in style, size, and thrust capabilities. Without doing a complete force analysis, it seemed doubtful that the ball screw actuator solution would be able to provide enough force in the horizontal direction to raise the seat lift mechanism. Weight would be comparable to the initial design, as the baseplate, carjack, and two rollers are removed, but two ball screw actuators are added.

Figure 18: Example of a Ball Screw Actuator [25].

A third solution involved a winch, roller bar, and damper spring. Considering the initial design, the two lower rollers would again be removed, but this time replaced with a roller bar (pinion) and slotted channel (rack). With a rack mounted on both sides of the frame, the pinion would be pulled by the winch (as seen in Figure 19) to raise the seat lift

mechanism and linkage system. Although this solution would probably work in the raising and lowering motions of the seat lift mechanism, there would need to be a method or device to counteract the winch. If there is any length of the winch cable released away from the housing, if the cable is not in tension, the seat lift system could be loose and not secured. In particular, if the winch has cable length released (the seat is in the lowered position), the seat would be able to be raised without much resistance since there is nothing counteracting that motion. Thus, a spring damper could be included.

Figure 19: Example of a Winch [26].

A spring damper (as seen in Figure 20) on the rear of the seat lift mechanism could prove very advantageous in this solution. Not only does it provide constant tension on the winch cable (whenever there is length released from the winch housing), the spring damper can act as a shock absorber, thus rendering the ride more comfortable. This spring damper would be fastened on both ends: one end to the seat lift mechanism and one end to the frame. That being said, there will be a large travel distance, which means a long extended position and a comparatively short home position. Research to find a spring damper that could fulfill this application was unsuccessful. This solution may be unstable if only one winch and one spring damper is used, as off-center loading may force the seat lift mechanism one way too far, which could damage the system. Weight and cost for this solution would be comparable to the other solutions.

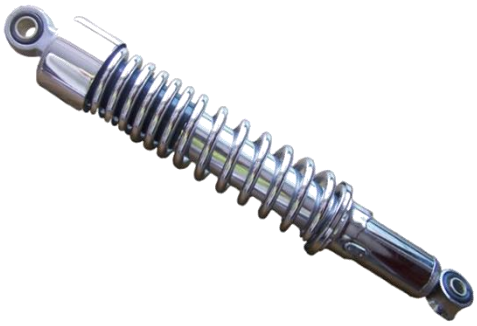

Figure 20: Example of a Spring Damper Shock Absorber [27].

The final solution concept incorporated a linear actuator, rack and pinion and roller bar, and linkage system. Mounted to the inside walls of the sides of the frame would be slotted plates that guide the roller bar. The roller bar would be fitted with a custom piece in the middle (its purpose explained next) and spur gears on the ends. These gears would replace the lower rollers from the initial design. This roller bar would rotate within these guide plates and racks on both sides.

The linear actuator (as seen in Figure 21) would be pinned to the rear vertical support of the frame. On the other end of the linear actuator is typically a through-hole in the shaft that travels out and back into the actuator housing. The custom piece, now resident to the roller bar (forced by the gears and guided by the slotted plates), could be fitted onto the end of the moving shaft (stroke) of the linear actuator. Utilizing the existing through-hole on that stroke, the custom piece could be fixed to the linear actuator's stroke (e.g., with a pin or screw). As the linear actuator extends its stroke, it pushes the custom piece, which pushes the roller bar, which rolls the gears, which raises the linkage system and seat lift mechanism. At any position between the linear actuator's minimum (recessed) and maximum (extended) positions, it would be able to remain locked in a position, and rolling prevention is supported by the rack and pinion gearing. The rack and pinion system also aids even and level lifting.

Figure 21: Example of a Linear Actuator [28].

Research was completed to find spur gears (pinions), gear tracks (racks), and a linear actuator. Similar to the spring damper from a prior solution, the difficult part in finding and choosing a linear actuator was its load and range capabilities. Weight and cost for this solution would be comparable to the other solutions. The overall comfort of the rider will be improved in the redesign based primarily on the new seat lift mechanism that was chosen – the last, including the linear actuator, rack and pinion and roller bar, and linkage system.

Additional storage for a second battery was a major concern voiced by many people who gave feedback. In the initial design of the Heliocycle, the battery was mounted between the rear vertical support of the frame and the rear wheel. This design proved functional, convenient, and reliable, but limiting. If a rider wanted to go for a long journey, storage for a secondary backup battery would be advisable. With most seat lift mechanism solutions consuming much of the inside space of the trike frame, two ideas were ideated.

The first option would be to store two batteries on top of the base of the frame, on either side of the rear vertical support. This design would be feasible, but it would also be very likely that the batteries would need to be removed from their mounting plates and swapped when necessary. The plug that gets inserted into the battery to connect to the

motor should not be left dangling or long; therefore, it should be minimized. In doing so, the plug should remain on one side of the trike; hence, the batteries would need to switch places for this solution to be safest.

A second, more efficient, method was ideated. If the battery-mounting plates are secured to the rear fork system, the two batteries can be mounted vertically, with their plug-receiving stabs pointed upwards. This way, the plug can be secured tightly to the frame, minimizing excess plug cable length. This method allows for the batteries to remain in their mounting plates the whole duration of the ride. Once the primary battery runs out of power, the plug can be switched to the secondary battery without physically swapping the batteries.

Storage for personal belongings was also improved in the redesign. In the initial design, there was a pouch secured underneath the seat. However, this was difficult to access, so the redesign features storage behind the seat instead of underneath it.

Redesign Model Development

A completely original CAD model was developed for this project. CAD that was completed for the initial design of the Heliocycle was done by Michael Caelwaerts in SolidWorks (see Figure 10 and Figure 11), whereas the CAD for this redesign was done completely new and in PTC Creo Parametric. In order to model the most accurate rendering, industry standard sizes were incorporated into the metal (aluminum) frame parts. Aside from the rollers, gears, and gear tracks (parts chosen on and taken from the McMaster-Carr website for accuracy), all of the trike parts were original CAD creations.

To complete the redesign rendering, it was first modeled after the existing prototype, and then modified to satisfy the redesign changes. For that reason, the CAD

model is very close to, if not already, to scale. No fasteners or welding features were included, which was done with the foresight that this slows the FEA computing time. Nevertheless, all assembled parts were mated with real-world connections (e.g., coincident, pin, translation, etc.). This allowed for animation of the seat lift mechanism to determine travel parameters. Not all animations were finalized, though, since not all real part files were acquired. The existing CAD model can be improved, though, once all real, off-the-shelf parts are selected. It would be ideal to incorporate their CAD models into this assembly (as what was done with the McMaster-Carr parts). For instance, the seat, wheels, chain, bogie wheels, crankset, and hardware (to name a few) can improve the accuracy of this CAD assembly. Meanwhile, renderings were created and assembled as best as possible, but they are acting as placeholders until authentic parts are acquired and included.

After careful consideration of the ideated solutions and multiple CAD revisions, a nearly complete rendering was produced in Creo, as seen in Figure 22 and Figure 23. A complete rendering would include authentic part files from vendors for any purchased, off-the-shelf parts, which would then be incorporated into the assembly. Since not every part's CAD file was obtained from a vendor, this assembly is nearly complete, but not fully complete.

Figure 22: A Front Isometric View of the Redesigned CAD Model.

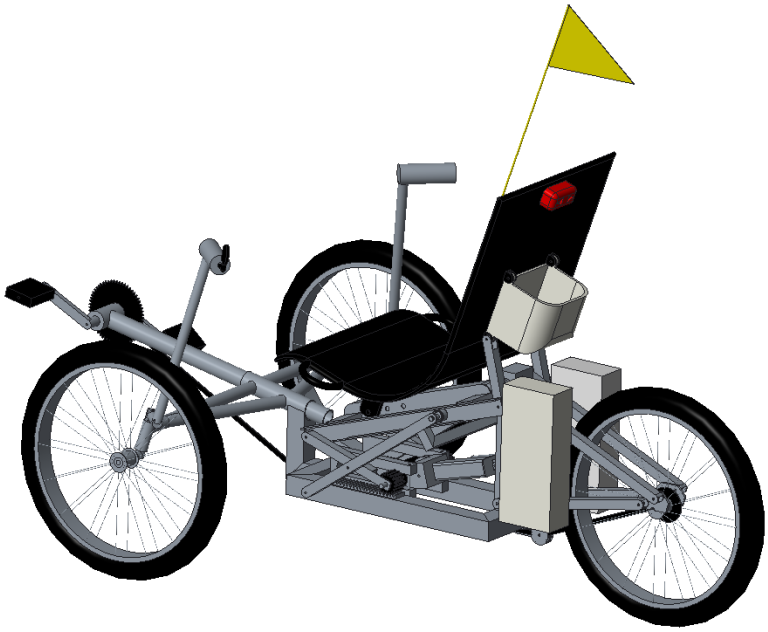

Figure 23: A Back Isometric View of the Redesigned CAD Model.

To make the redesigned Heliocycle lighter in weight, aluminum was chosen as the base structural metal (instead of mild steel – which was used in the original Heliocycle build). Industry standards for channel, plate, rectangular tube, round pipe, round tube, and

square tube were used in the design. Aluminum is typically 2.5 times less dense than steel, and aluminum can offer good corrosion resistance [29]. Both of these characteristics are favorable in this application. Furthermore, aluminum can be more malleable and elastic compared to steel [29], which could make the frame more forgiving to road imperfections, thus make the riding more comfortable. Fabricating with aluminum can be more difficult than with steel, especially when welding, and depending on the supply and demand of the world, cost could become an issue, too. Nevertheless, aluminum 6061-T6 was chosen as the base material for this project, which is a common alloy used in manufacturing.

A stripped-down version of the redesigned frame only can be seen in Figure 24, Figure 25, and Figure 26. Each figure in the progression of this three-figure series has subassemblies added to show the different stages of assembling the frame.

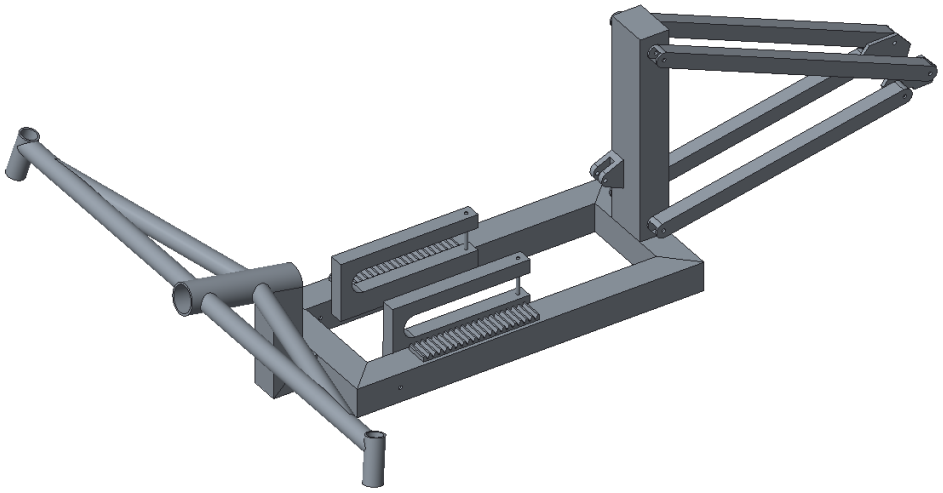

Figure 24: An Isometric View of the Redesigned Frame – Stage 1/3.

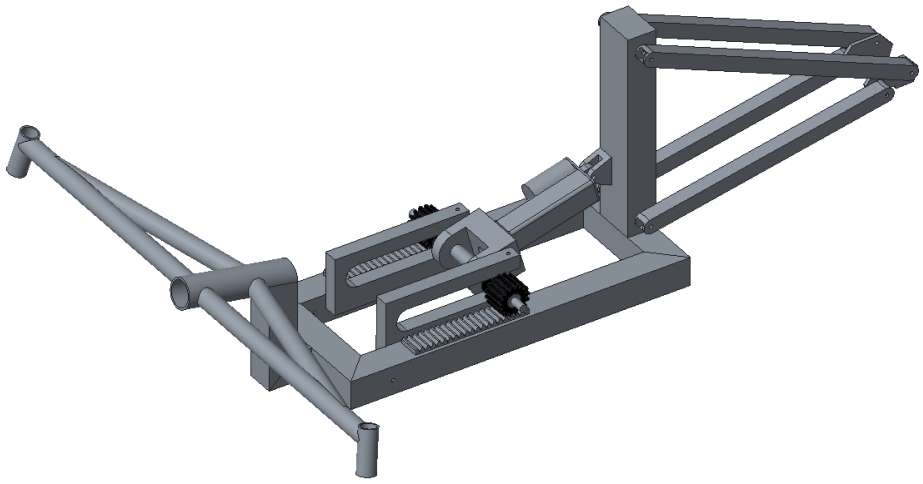

Figure 25: An Isometric View of the Redesigned Frame – Stage 2/3.

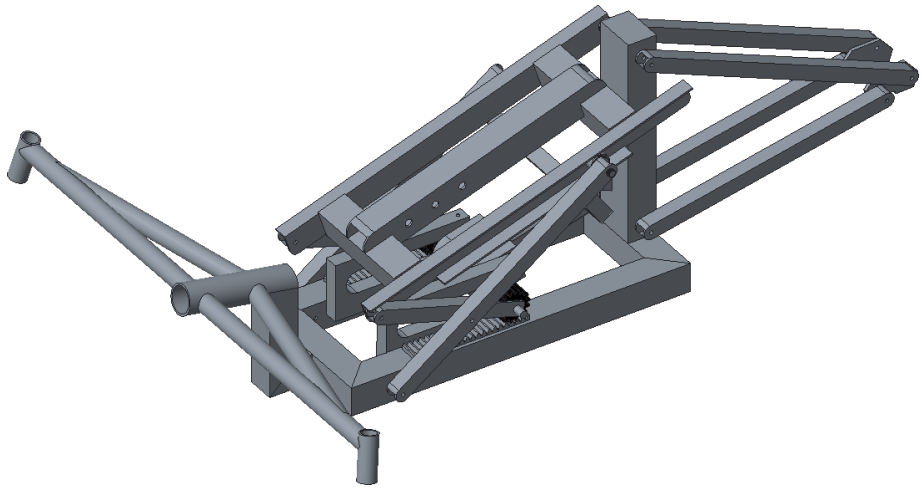

Figure 26: An Isometric View of the Redesigned Frame – Stage 3/3.

Stage 1/3 of the frame build serves as the baseline on which the other subassemblies get built onto. This stage is comprised of the rectangular base subassembly, the gooseneck subassembly, the front boom subassembly, and the rear subassembly. In Stage 2/3 of the frame build, the linear actuator and gear/roller subassemblies get added to the frame. In Stage 3/3 of the frame build, the seat assist mechanism subassembly gets added. This completes the frame portion of the trike. However, to complete the finite element analysis on the frame, this was modified (for reasons explained later).

Handles (from gathered feedback, and separate from the steering handles atop the steering tillers) were designed directly into the seat frame. It was determined to mount the handles directly into the seat frame – versus into the seat lifting mechanism base – because the placement would be beneficial closer to the rider's hips instead of being farther away. Provided that the target audience is anticipated to have limited mobility, having the handles closer would require less range of motion. The inclusion of the handles is shown in Figure 27 (left). The seat was also designed with brackets underneath and in back, as shown in Figure 27 (right). Underneath the seat is the large bracket, which is the front mounting location for the seat to the seat lift mechanism. The back of the seat has four brackets: the upper two brackets are for the top of the personal essentials basket to mount to, and the lower two brackets are for the seat to mount to the seat lift mechanism in the rear, as well as to serve as the lower mounting location for the personal essentials basket.

Figure 27: Views of the Seat Handles (left) and Mounting Brackets (right).

Additional storage for a secondary backup battery was implemented by mounting two batteries vertically on the rear fork system, as seen in Figure 28 (left). Another view of the additional battery storage is shown in Figure 28 (right), but this image shows the rear subassembly with the batteries removed and their mounting plates remaining. This was utilized in the finite element analysis. More storage space was included with the addition of the compartment fastened to the back of the seat.

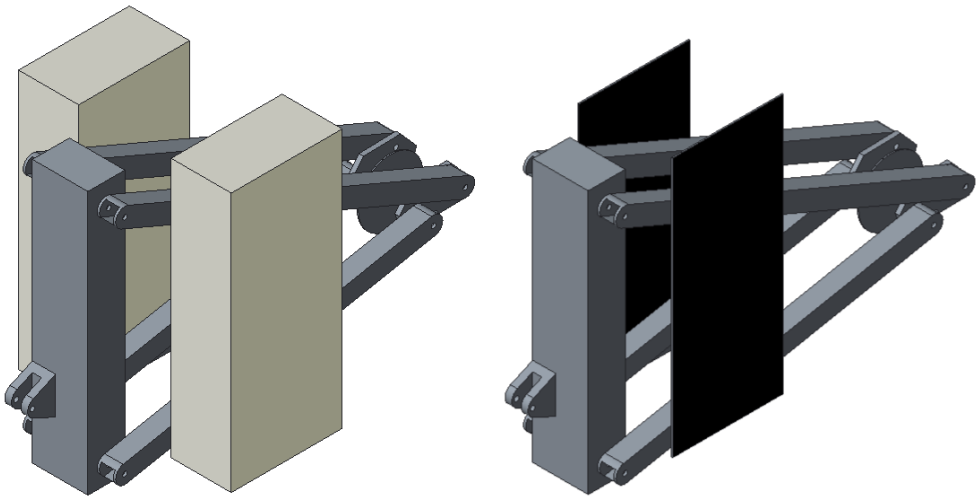

Figure 28: Rear Fork Assembly with Two Batteries (left) or Two Battery Plates (right).

The seat lift mechanism was drastically changed. Compared to the initial design, the baseplate and carjack device were removed, as well as the lower rollers. The last solution that was discussed in the Idea Generation section was the design that was selected for implementation. That being said, the initial linkage system was combined with a linear actuator, custom connector, roller bar, and a rack and pinion system (gear and gear track and slotted plates). The upper rollers (at the opposite end of the pinned, longer linkage arms) remained in the redesign. A close-up of the new seat lift mechanism can be seen in Figure 29 and Figure 30, whereas an overall right side view of the trike in its lowered and raised positions can be seen in Figure 31 and Figure 32, respectively.

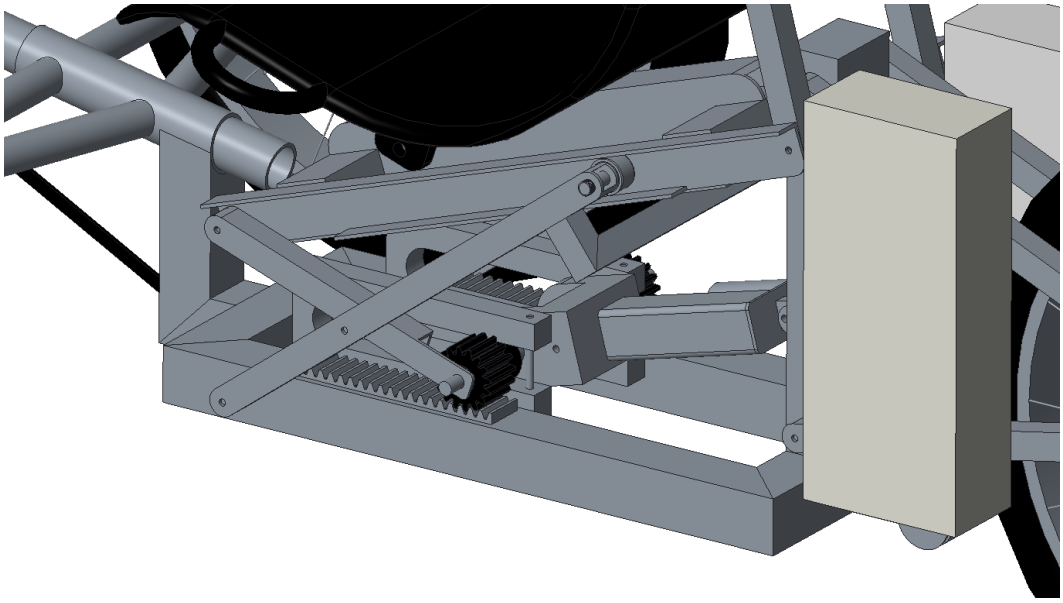

Figure 29: Close-up of the Redesigned Seat Lift Mechanism, Lowered/Retracted.

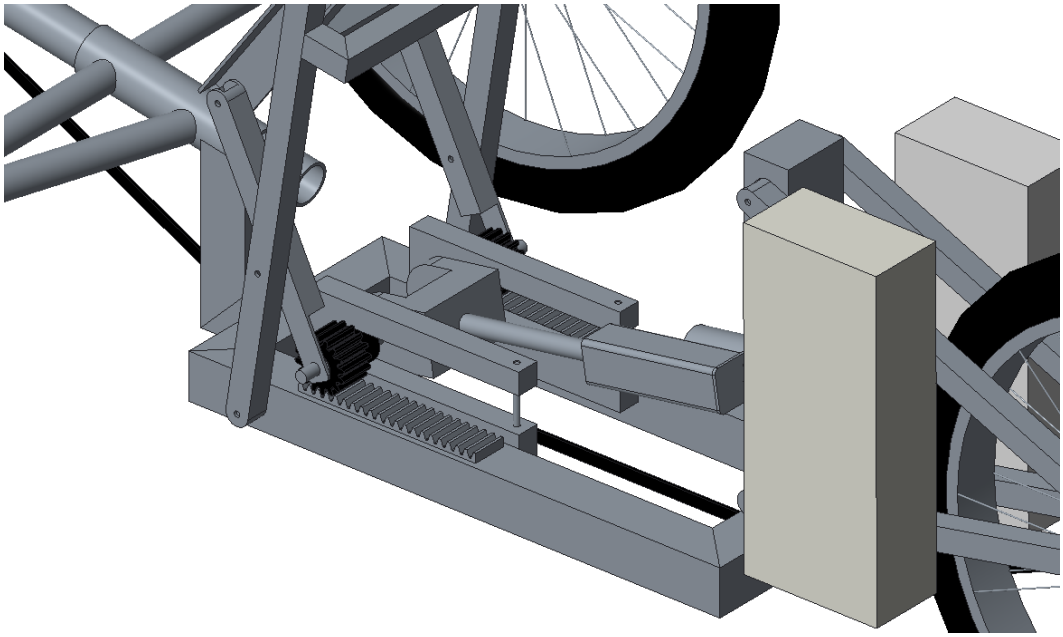

Figure 30: Close-up of the Redesigned Seat Lift Mechanism, Raised/Extended.

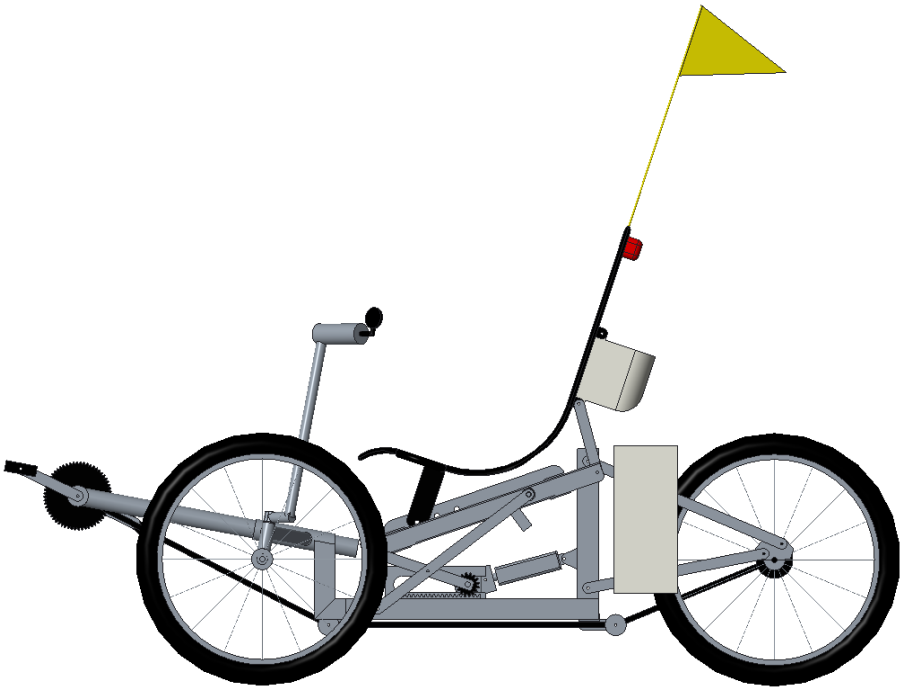

Figure 31: Side View of Redesigned Heliocycle in Lowered Position.

Figure 32: Side View of Redesigned Heliocycle in Raised Position.

The slotted plates have an open slot to be able to insert the roller bar, but then have the ability to receive a fastener to close the opened slot, which can be seen in Figure 30. This model can be made more realistic once the authentic CAD file from the vendor is implemented. To be able to complete the analysis portion of this project, the Progressive Automations Model PA-03-6-600 Linear Actuator was chosen. This actuator has a 6-in. stroke, can exert a force of 600 lb_f, travels at 0.39 ips, and features an input voltage of 12 V DC and has a full load current of 7.6 A, thus making this option a 91.2 W output-capable actuator [30]. Considerations included but were not limited to: retracted and extended lengths, maximum allowable load, travel speed, and input voltage. It would be ideal to have the input voltage of the linear actuator match that of the battery's voltage. If the two match, no further work would be necessary – otherwise, a voltage converter would be needed (which adds cost, weight, and complexity). At this time, however, the two voltages do not match, so a voltage converter would be needed.

The CAD files for the redesigned trike satisfy the feedback suggestions. Going forward, the CAD assemblies could be improved by including realistic parts that would be used if the Heliocycle were to be rebuilt. Then, engineering analysis could be redone and may be more true to any real-world builds.

Engineering Analysis

The engineering analysis for this project was broken up into three sections: factor of safety (FOS) determination, gear stress analysis, and finite element analysis of the frame. This analysis was completed using various methods and technologies, which are described in detail in their respective sections. The FOS determination and gear stress analysis calculations were performed in MATLAB (code can be found in Appendix B).

Factor of Safety Determination

The FOS was determined using the Pugsley Method. This method takes into account five different characteristics that are broken up into two categories and tables, recreated in Table 4 and Table 5, which are used to determine N_1 and N_2. When N_1 and N_2 are determined, their product is the resulting Pugsley Method factor of safety, N [31].

Table 4: Pugsley Method Values for Safety Factor Characteristics to Determine N1 [31].

Characteristic		B = VG	B = G	B = F	B = P
A = VG	C = VG	1.10	1.30	1.50	1.70
	C = G	1.20	1.45	1.70	1.95
	C = F	1.30	1.60	1.90	2.20
	C = P	1.40	1.75	2.10	2.45
A = G	C = VG	1.30	1.55	1.80	2.05
	C = G	1.45	1.75	2.05	2.35
	C = F	1.60	1.95	2.30	2.65
	C = P	1.75	2.15	2.55	2.95
A = F	C = VG	1.50	1.80	2.10	2.40
	C = G	1.70	2.05	2.40	2.75
	C = F	1.90	2.30	2.70	3.10
	C = P	2.10	2.55	3.00	3.45
A =P	C = VG	1.70	2.15	2.40	2.75
	C = G	1.95	2.35	2.75	3.15
	C = F	2.20	2.65	3.10	3.55
	C = P	2.45	2.95	3.45	3.95

Table 5: Pugsley Method Values for Safety Factor Characteristics to Determine N2 [31].

Characteristic	E = NS	E = S	E = VS
D = NS	1.0	1.0	1.2
D = S	1.2	1.3	1.4
D = VS	1.4	1.5	1.6

In Table 4 and Table 5, the five characteristics – A, B, C, D, and E – are determined by the engineer. For Table 4, the A characteristic represents the quality of materials, workmanship, maintenance, and inspection, B is the control over applied loads, and C is the accuracy of the stress analysis, experimental data, or experience with similar parts. These three characteristics are rated on the scale of VG (very good), G (good), F

(fair), and P (poor). As for Table 5, D represents the danger to people, and E is the economic impact. These two characteristics are rated on the scale of VS (very serious), S (serious), and NS (not serious). When there is uncertainty in deciding, oftentimes a conservative estimate is made.

For this project, it was decided that A = VG, C = G, and B = G, thus resulting in $N_1 = 1.45$. Also, it was decided that D = S, and E = S, thus resulting in $N_2 = 1.3$. Because $N_1 = 1.45$ and $N_2 = 1.3$, their product equates to N = 1.885, which was rounded up to the nearest whole number. That being said, the factor of safety for the project is two (N = 2).

With the factor of safety for this project determined, the maximum design load could be adjusted. The stated design constraint for the maximum rider size of 300 lb_m was therefore scaled up N times, resulting in the maximum design load to be 600 lb_m. Using the following force equals mass times acceleration (F = ma) conversion, this mass can be converted into a force [32]:

$$\left[1\ \mathrm{lb_m}\left(\frac{1\ \mathrm{slug}}{32.2\ \mathrm{lb_m}}\right)\right]\left(32.2\ \frac{\mathrm{ft}}{\mathrm{s^2}}\right) = 1\ \mathrm{lb_f}. \quad (1)$$

The maximum design load is therefore equivalent to 600 lb_f, which is almost 2670 N (2668.93 N to be more exact). This 2670 N maximum load was used as a maximum force in FEA in subsequent analysis.

Gear Stress Analysis – Component Properties

Before completing the gear stress analysis, the dimensions and properties of the selected linear actuator and gear first had to be established. As previously mentioned, the linear actuator (Progressive Automations Model PA-03-6-600 Linear Actuator) had a stroke length of 6 in., force capacity of 600 lb_f, speed of 0.39 ips, input voltage of 12 V

DC, full load current of 7.6 A, and power delivery of 91.2 W [30]. This power was converted to 0.122 hp, or 807.2 ft·lb_f/s.

The gear that was chosen (McMaster-Carr part number 5172T42) did not have a published material code or type; documentation indicated that it was steel [33]. Therefore, research was conducted [34] to determine that many gears are made from a medium carbon steel [35], namely, steel code AISI 1050 [36]. Hence, AISI 1050 was assumed to be the material that 5172T42 was made from. This assumption was made to be able to get material properties from the MatWeb Material Property Data website at http://www.matweb.com/.

From McMaster-Carr's published information online, 5172T42 has a diametral pitch (P_d) of 8 teeth/in, a total number of teeth (N_p) of 16, a pitch diameter (d_p) of 2 in, a pitch radius (r_p) of 1 in, a face width (F) of 1.5 in, and pressure angle (PA or Φ) of 20 degrees [33].

From MatWeb online, AISI 1050 has the properties displayed in Table 6.

Table 6: Properties of AISI 1050 in English Units and SI Units [37].

Property	Symbol	English		SI	
		Dimension	Unit	Dimension	Unit
Density	ρ	0.284	lbm/in³	7.87	g/cm³
Hardness, Brinell	H_B	170	HB	170	HB
Tensile Strength, Ultimate	S_{ut}	84,800	psi	585	MPa
Tensile Strength, Yield	S_y	74,700	psi	515	MPa
Modulus of Elasticity	E	29.0E+06	psi	200	GPa
Bulk Modulus	K	23.2E+06	psi	160	GPa
Poisson's Ratio	ν	0.29	-	0.29	-
Shear Modulus	G	11.6E+06	psi	80.0	GPa
Coefficient of Thermal Expansion	CTE	6.39E-06	in/(in·°F)	11.5E-06	m/(m·°C)
Specific Heat Capacity	C_p	0.116	BTU/(lb·°F)	0.486	J/(g·°C)
Thermal Conductivity	k	360	(BTU·in)/(hr·ft²·°F)	51.9	W/(m·K)

The properties shown in Table 6 were needed to complete the gear stress and finite element analyses. In particular, the English units were used in the gear stress analysis, and their International System (SI) unit equivalents were used in the FEA.

Before the bending stress was calculated, a few characteristics of the system were calculated. The angular velocity of the gear (ω) was calculated knowing the pitch radius (r_p) and linear velocity (v):

$$\omega = \frac{v}{r_p} = \left(\frac{0.39\,\frac{\text{in.}}{\text{s}}}{1\,\frac{\text{in.}}{\text{rot}}}\right)\left(\frac{1\text{ rev}}{1\text{ rot}}\right)\left(\frac{60\text{ s}}{1\text{ min}}\right) = 23.4\text{ rpm}, \tag{2}$$

which was then converted into metric units (rad/s):

$$\omega_m = \left(23.4\,\frac{\text{rev}}{\text{min}}\right)\left(\frac{2\pi\text{ rad}}{1\text{ rev}}\right)\left(\frac{1\text{ min}}{60\text{ s}}\right) = 2.45\,\frac{\text{rad}}{\text{s}}. \tag{3}$$

The torque on the pinion (T_p) [21] was calculated as the power exerted by the linear actuator (H_2) divided by the pinion angular velocity (ω_m):

$$T_p = \frac{H_2}{\omega_m} = \frac{807.2\,\frac{\text{ft}\cdot\text{lb}_\text{f}}{\text{s}}}{2.45\,\frac{\text{rad}}{\text{s}}} = 329.4\text{ ft}\cdot\text{lb}_\text{f}. \tag{4}$$

Gear Stress Analysis – Bending Stress

In order to complete the gear stress analysis, the Tenth Edition of *Shigley's Mechanical Engineering Design* textbook was referenced and used exclusively throughout this portion of the project's analysis [21]. That being said, all of the equations used in this section – Equation (5) through Equation (26) – were derived or taken from this textbook [21]. According to this book, there are two major ways a gear can fail – as a result of excessive bending stress or excessive contact stress (also called pitting resistance). First, bending stress calculations were made to determine if the chosen gear under the prescribed loads would fail.

In order to calculate the bending stress, the following formula was used:

$$\sigma_b = W^t K_o K_v K_s \frac{P_d}{F} \frac{K_m K_B}{J}, \tag{5}$$

where W^t is the tangential transmitted load (lb_f), K_o is the overload factor, K_v is the dynamic factor, K_s is the size factor, P_d is the transverse diametral pitch, F is the face width of the narrower member (in), K_m is the load-distribution factor, K_B is the rim-thickness factor, and J is the geometry factor for bending strength (which includes the root fillet stress-concentration factor K_f).

The tangential transmitted load was determined using the following equation:

$$W^t = 33{,}000 \frac{H}{V} = 33{,}000 \left(\frac{0.122 \text{ hp}}{12.3 \text{ fpm}}\right) = 329.4 \text{ lb}_\text{f}, \tag{6}$$

where H is the power (previously found to be 0.122 hp), and V is the pitch-line velocity, which was determined using the following equation:

$$V = \frac{\pi \, d_p \, \omega}{12} = \frac{(\pi)(2 \text{ in.})(23.4 \text{ rpm})}{\frac{12 \text{ in.}}{1 \text{ ft}}} = 12.3 \text{ fpm}. \tag{7}$$

The overload factor was neglected (K_o = 1) because externally applied loads are not in excess of the nominal tangential load in a particular application. Furthermore, the power source is assumed to be uniform/uniform, which indicates K_o = 1.

The dynamic factor was determined using the following equation:

$$K_v = \left(\frac{K_{v,A} + \sqrt{V}}{K_{v,A}}\right)^{K_{v,B}} = \left(\frac{45.4 + \sqrt{12.3}}{45.4}\right)^{1.1} = 1.0836, \tag{8}$$

where $K_{v,A}$ and $K_{v,B}$ are dynamic factor constants, and defined as:

$$K_{v,A} = 50 + 56\left(1 - K_{v,B}\right) = 50 + 56(1 - 1.1) = 45.4, \tag{9}$$

$$K_{v,B} = 0.25\left(12 - K_{v,Q_v}\right)^{2/3} = 0.25(12 - 3)^{2/3} = 1.1, \tag{10}$$

where Q_v is defined as a quality number. The AGMA defined a set of quality numbers that are associated with gears, and they "define the tolerances for gears of various sizes manufactured to a specified accuracy" [21]. Since the quality number for gear 5172T42 was not published, the worst case scenario of 3 was assumed (on a whole-number scale from 3 to 12, where 3 to 7 include most commercial quality gears, and where 8 to 12 are for precision quality).

The size factor was determined using the following equation:

$$K_s = 1.192\left(\frac{F\sqrt{Y}}{P_d}\right)^{0.0535} = 1.192\left(\frac{(1.5\text{ in.})\sqrt{0.296}}{8\text{ in.}}\right)^{0.0535} = 1.0550, \quad (11)$$

where Y is the Lewis Form Factor. Since the number of teeth on the gear (N_p) is 16, the Lewis Form Factor is 0.296.

The load-distribution factor was determined using the following equation:

$$K_m = 1 + C_{mc}\left(C_{pf}C_{pm} + C_{ma}C_e\right) = 1 + 1[0.06(1) + 0.27(1)] = 1.3281, \quad (12)$$

where the constants were chosen based on scenarios specific to each constant. The constant C_{mc} was defined as 1 since the gear teeth are uncrowned. Since F is 1.5 in, C_{pf} was determined using the following equation:

$$C_{pf} = \frac{F}{10d_p} - 0.0375 + 0.0125F = \frac{1.5\text{ in.}}{10(2\text{ in.})} - 0.0375 + 0.0125(1.5) = 0.06. \quad (13)$$

Furthermore, C_{pm} was neglected (C_{pm} = 1) since bearings and a shaft were not parts of this portion of the design. Next, the C_{ma} factor was determined using the following equation:

$$C_{ma} = C_{ma,A} + C_{ma,B}F + C_{ma,C}F^2, \quad (14)$$

where the empirical constants ($C_{ma,A}$, $C_{ma,B}$, and $C_{ma,C}$) were taken from a table in Shigley (p.752) for the open gearing condition and substituted into the C_{ma} equation:

$$C_{ma} = 0.247 + 0.0167(1.5) - 0.765(10^{-4})(1.5)^2 = 0.27. \quad (15)$$

The factor C_e was one of two options, either a value of 0.8 "for gearing adjusted at assembly, or compatibility is improved by lapping, or both," or a value of 1 "for all other conditions" [21]. Since the first condition (for a value of 0.8) did not satisfy this application, a value of 1 was assigned to C_e.

The rim-thickness factor was determined after the backup ratio (m_B) was calculated:

$$m_B = \frac{t_R}{h_t} = \frac{0.417875 \text{ in.}}{0.269625 \text{ in.}} = 1.5498 \geq 1.2, \quad (16)$$

where t_R is the gear's rim thickness and h_t is the gear's tooth height. These two values were measured directly on the authentic CAD file of the gear. Since m_B was found to be greater than 1.2, K_B is neglected ($K_B = 1$). The K_B factor would have been a different value if m_B was less than 1.2.

The AGMA bending-strength geometry factor was determined using the following equation:

$$J = \frac{Y}{K_f m_N} = \frac{0.296}{1(1.0)} = 0.296, \quad (17)$$

where K_f is the fatigue stress-concentration factor and m_N is the load-sharing ratio. The K_f factor is dependent on notches, and it was assumed there were no notches in the gear, so K_f was neglected ($K_f = 1$). Also, m_N is neglected for spur gears ($m_N = 1.0$ for spur gears). Thus, the AGMA bending-strength geometry factor is simply the Lewis Form Factor value.

Knowing all these values, the bending stress was calculated using the following equation:

$$\sigma_b = W^t K_o K_v K_s \frac{P_d}{F} \frac{K_m K_B}{J} = (329.4 \text{ lb}_\text{f})(1)(1.0836)(1.0550)\left(\frac{8 \text{ in.}}{1.5 \text{ in.}}\right)\left(\frac{1.321(1)}{0.296}\right) = 9012 \text{ psi}. \quad (18)$$

With the bending stress known, the allowable bending stress was determined two different ways, using the following equations:

$$\sigma_{b,allow,1} = \frac{S_y}{N} = \frac{74{,}700 \text{ psi}}{2} = 37{,}350 \text{ psi}, \tag{19}$$

$$\sigma_{b,allow,2} = \sigma_b \, S_{F,b} = (9012 \text{ psi})(4.2282) = 38{,}102 \text{ psi}, \tag{20}$$

where $S_{F,b}$ is the AGMA factor of safety of a gear in bending (also called a stress ratio), which was found using the following equation:

$$S_{F,b} = \frac{S_t Y_N/(K_T K_R)}{\sigma_b} = \frac{(25{,}941 \text{ psi})(1.2485)/[(1)(0.85)]}{9{,}012 \text{ psi}} = 4.2282. \tag{21}$$

The gear bending stress (S_t) was found using a figure and resident line of best fit equation, knowing the Brinell hardness (H_B) of AISI 1050 and choosing its material grade, assuming the worst case scenario (Grade 1). Thus,

$$S_t = 77.3H_B + 12{,}800 = 77.3(170) + 12{,}800 = 25{,}941 \text{ psi}. \tag{22}$$

The stress-cycle factor (Y_N) was also derived from a figure and resident line of best fit equation, but also prescribing the goal number of cycles desired for the gear's life (N_C) being 10^4 cycles. The reasoning behind choosing this quantity of N_C will be discussed in the section detailing the gear contact stress analysis. Another contributing factor that went into deciding which trendline equation to use involved the hardness of AISI 1050. Since 170HB did not have an equation, the next closest was 160HB, so that equation was chosen and used:

$$Y_N = 2.3194 \, N_C^{-0.0538} = 2.3194(10^4)^{-0.0538} = 1.2485. \tag{23}$$

The temperature factor was neglected (K_T = 1.0) since the operating temperature is assumed to always be below 250°F. The reliability factor (K_R) was chosen to be 0.85 because this was based on the reliability (R) being selected as 0.90. The reliability of the gear material was not published, so this value was chosen. Typical reliabilities range

from 0.90 to 0.99, but the reliability can be above or below this range (but not exceed 1). The value of 0.90 was chosen as a typical but conservative reliability.

Since there were two different allowable bending stresses calculated, two different factors of safety were calculated:

$$S_{F,b,1} = \frac{\sigma_{b,allow,1}}{\sigma_b} = \frac{37{,}350 \text{ psi}}{9{,}012 \text{ psi}} = 4.1448, \tag{24}$$

$$S_{F,b,2} = \frac{\sigma_{b,allow,2}}{\sigma_b} = \frac{38{,}102 \text{ psi}}{9{,}012 \text{ psi}} = 4.2282. \tag{25}$$

Note: the value of $S_{F,b}$ in Equation (21) is equivalent to $S_{F,b,2}$ in Equation (25). To find the approximate factor of safety for bending stress, the average of the two factors of safety was calculated:

$$S_{F,b,avg} = \frac{S_{F,b,1} + S_{F,b,2}}{2} = \frac{4.1448 + 4.2282}{2} = 4.1865. \tag{26}$$

Concluding this portion of the analysis, since the factor of safety for bending stress is greater than one, the gear is safe from failing due to bending stress.

Gear Stress Analysis – Contact Stress (Pitting Resistance)

Completing the gear stress analysis for contact stress did not take as many steps as the gear stress analysis for bending stress because several characteristics carried over from bending into contact calculations. Again, in order to complete the gear stress analysis, the Tenth Edition of *Shigley's Mechanical Engineering Design* textbook was referenced and used exclusively throughout this portion of the project's analysis [21]. That being said, all of the equations used in this section – Equation (27) through Equation (34) – were derived or taken from this textbook [21]. The contact stress was determined using the following equation:

$$\sigma_c = C_P \sqrt{W^t K_o K_v K_s \frac{K_m}{d_p F} \frac{C_f}{I}}, \tag{27}$$

where C_P is the elastic coefficient (√psi), C_f is the surface condition factor, d_p is the pitch diameter of the pinion (in), and I is the geometry factor for pitting resistance.

The elastic coefficient (C_P, not to be confused with the specific heat variable C_p) was determined using the following equation:

$$C_P = \left[\frac{1}{\pi\left(\frac{1-\nu_p^2}{E_p}+\frac{1-\nu_G^2}{E_G}\right)}\right]^{1/2} = \left[\frac{1}{2\pi\left(\frac{1-\nu^2}{E}\right)}\right]^{1/2} = \left[\frac{1}{2\pi\left(\frac{1-(0.29)^2}{29.0\text{E+06 psi}}\right)}\right]^{1/2} = 2{,}245\ (\text{psi})^{1/2}. \quad (28)$$

The equation for the elastic coefficient was simplified because the materials in the pinion and gear (rack) are the same.

The surface condition factor was neglected (C_F = 1) because no surface conditions were published or known.

Next, the surface-strength geometry factor (also called the pitting-resistance geometry factor) for external spur gears was determined using the following equation:

$$I = \frac{\cos\phi_t \sin\phi_t}{2m_N}\frac{m_G}{m_G+1} = \frac{\cos 20^\circ \sin 20^\circ}{2(1)}\frac{1}{1+1} = 0.0803, \quad (29)$$

where the transverse pressure angle (Φ_t) was found by the following equation:

$$\phi_t = \tan^{-1}\left(\frac{\tan(\phi_n)}{\cos(\psi)}\right) = \tan^{-1}\left(\frac{\tan(20^\circ)}{\cos(0^\circ)}\right) = 20^\circ. \quad (30)$$

The transverse pressure angle includes trigonometric functions of two more angles, the normal pressure angle (Φ_n) and the helix angle (Ψ). For spur gears, the normal pressure angle is equal to the pressure angle and the helix angle is zero. Continuing, the gear speed ratio (m_G) is the ratio of the number of teeth on the gear compared to the number of teeth on the pinion. Since this system utilizes a rack and pinion system, the number of teeth on the gear (rack) was set equal to the number of teeth on the pinion; thus, the ratio of the number of teeth was set equal to one.

Knowing all these values, the contact stress was calculated using the following equation:

$$\sigma_c = \left(2245\ (\text{psi})^{\frac{1}{2}}\right)\sqrt{(329.4\ \text{lb}_\text{f})(1)(1.0836)(1.0550)\frac{1.3281}{(2\ \text{in.})(1.5\ \text{in.})}\frac{1}{0.0803}} = 102{,}253\ \text{psi}. \quad (31)$$

With the contact stress known, the allowable contact stress was determined using the following equation:

$$\sigma_{c,allow} = \sigma_c\, S_{H,c} = (102{,}253\ \text{psi})(1.2484) = 127{,}652\ \text{psi}, \quad (32)$$

where $S_{H,c}$ is the wear factor of safety. This factor of safety for contact stress was found using the following equation:

$$S_{H,c} = \frac{S_c Z_N C_H/(K_T K_R)}{\sigma_c} = \frac{(83{,}840\ \text{psi})(1.2942)(1)/[(1.0)(0.85)]}{102{,}253\ \text{psi}} = 1.2484, \quad (33)$$

where S_c is the allowable contact stress number (which is also called the contact-fatigue strength). This parameter was found using a figure and resident line of best fit equation, knowing the Brinell hardness of AISI 1050 and choosing its material grade, assuming the worst case scenario (Grade 1):

$$S_c = 322H_B + 29{,}100 = 322(170) + 29{,}100 = 83{,}840\ \text{psi}. \quad (34)$$

The pitting resistance stress-cycle factor (Z_N) was also derived from a figure and resident line of best fit equation, but also prescribing the goal number of cycles desired for the gear's life being 10^4 cycles. After running several iterations to calculate the bending and contact stresses, their allowable stresses, and their factors of safety, it was found that 10^4 cycles was the most cycles when inputting 10^n cycles (for n = 0, 1, 2, …) and ensuring the factors of safety did not result in anything less than one. In other words, when 10^5 cycles was selected for N_C, the factor of safety for contact stress was very close to or less than one; thus, 10^4 cycles was prescribed for this analysis and project to be

conservative. Lastly, the hardness-ratio factor was neglected ($C_H = 1$), since this factor is used only for the gear and this analysis examined the pinion (and $C_H = 1$ for the pinion).

Concluding this portion of the analysis, since the factor of safety for contact stress is greater than one, the gear is safe from failing due to contact stress. Nevertheless, it is worth noting that the calculated and allowable contact stress both exceed the AISI 1050 ultimate tensile strength and yield tensile strength.

Finite Element Analysis of Frame – Preliminary

In order to complete the finite element analysis of the frame, the entire CAD assembly of the trike was first completed, and then it was stripped down to just the frame components. As mentioned previously, the frame assembly that was used to complete the FEA was slightly modified from the one shown in Figure 26. More specifically, the seat was included (plus its two tubular support members behind it), but the racks (parts of the rack and pinion systems) were excluded – for reasons explained later. Also, the gears were replaced by cylinders that featured hub diameters and overall widths equivalent to the gears (intended to simplify meshing and reduce computation time as a result of fewer features). Furthermore, it was determined that the batteries did not offer much structural support, so they were removed from the frame assembly to complete the FEA. However, their mounting plates remained.

Two different FEA runs were completed – one for the lowered position (when the linear actuator is retracted and the seat is lowered) and one for the raised position (when the linear actuator is extended and the seat is raised). This FEA was completed in ANSYS 17.2 (Workbench) and using Static Structural Analysis System. Since the two FEA runs used the same materials, the Engineering Data for these materials were entered

into the A-Project and then linked to the B-Project. The Engineering Data were populated with data sourced from MatWeb for the two materials found in the frame: AISI 1050 steel [37] and aluminum 6061-T6 [38]. The ANSYS default material of Structural Steel was duplicated and modified with known properties of AISI 1050 (see Figure 33), and the ANSYS default material of Aluminum Alloy was duplicated and modified with known properties of aluminum 6061-T6 (see Figure 34).

Outline of Schematic A2: Engineering Data

	A	B	C	D	E
1	Contents of Engineering Data			Source	Description
2	Material				
3	AISI 1050 Steel (modified Structural Steel)			General_Materials.xml	Fatigue Data at zero mean stress comes from 1998 ASME BPV Code, Section 8, Div 2, Table 5-110.1
4	Aluminum 6061-T6 (modified Aluminum Alloy)			General_Materials.xml	General aluminum alloy. Fatigue properties come from MIL-HDBK -5H, page 3-277.
*	Click here to add a new material				

Properties of Outline Row 3: AISI 1050 Steel (modified Structural Steel)

	A	B	C	D	E
1	Property	Value	Unit		
2	Density	7870	kg m^-3		
3	Isotropic Secant Coefficient of Thermal Expansion				
4	Coefficient of Thermal Expansion	1.15E-05	C^-1		
5	Zero-Thermal-Strain Reference Temperature	22	C		
6	Isotropic Elasticity				
7	Derive from	Young's Modulus and Poisson's Ratio			
8	Young's Modulus	2E+11	Pa		
9	Poisson's Ratio	0.29			
10	Bulk Modulus	1.5873E+11	Pa		
11	Shear Modulus	7.7519E+10	Pa		
12	Alternating Stress Mean Stress	Tabular			
13	Interpolation	Log-Log			
14	Scale	1			
15	Offset	0	Pa		
16	Strain-Life Parameters				
17	Display Curve Type	Strain-Life			
18	Strength Coefficient	9.2E+08	Pa		
19	Strength Exponent	-0.106			
20	Ductility Coefficient	0.213			
21	Ductility Exponent	-0.47			
22	Cyclic Strength Coefficient	1E+09	Pa		
23	Cyclic Strain Hardening Exponent	0.2			
24	Tensile Yield Strength	5.15E+08	Pa		
25	Compressive Yield Strength	5.15E+08	Pa		
26	Tensile Ultimate Strength	5.85E+08	Pa		
27	Compressive Ultimate Strength	0	Pa		

Figure 33: Engineering Data for AISI 1050 Steel [37].

Outline of Schematic A2: Engineering Data

	A	B	C	D	E
1	Contents of Engineering Data			Source	Description
2	Material				
3	AISI 1050 Steel (modified Structural Steel)			General_Materials.xml	Fatigue Data at zero mean stress comes from 1998 ASME BPV Code, Section 8, Div 2, Table 5-110.1
4	Aluminum 6061-T6 (modified Aluminum Alloy)			General_Materials.xml	General aluminum alloy. Fatigue properties come from MIL-HDBK -5H, page 3-277.
*	Click here to add a new material				

Properties of Outline Row 4: Aluminum 6061-T6 (modified Aluminum Alloy)

	A	B	C	D	E
1	Property	Value	Unit		
2	Density	2700	kg m^-3		
3	Isotropic Secant Coefficient of Thermal Expansion				
4	Coefficient of Thermal Expansion	2.36E-05	C^-1		
5	Zero-Thermal-Strain Reference Temperature	22	C		
6	Isotropic Elasticity				
7	Derive from	Young's Modulus and Poisson's Ratio			
8	Young's Modulus	6.89E+10	Pa		
9	Poisson's Ratio	0.33			
10	Bulk Modulus	6.7549E+10	Pa		
11	Shear Modulus	2.5902E+10	Pa		
12	Alternating Stress R-Ratio	Tabular			
13	Interpolation	Semi-Log			
14	Scale	1			
15	Offset	0	Pa		
16	Tensile Yield Strength	2.76E+08	Pa		
17	Compressive Yield Strength	2.76E+08	Pa		
18	Tensile Ultimate Strength	3.1E+08	Pa		
19	Compressive Ultimate Strength	0	Pa		

Figure 34: Engineering Data for Aluminum 6061-T6 [38].

Finite Element Analysis of Frame – Lowered Position Setup

One finite element analysis examined the lowered position, as seen in Figure 35.

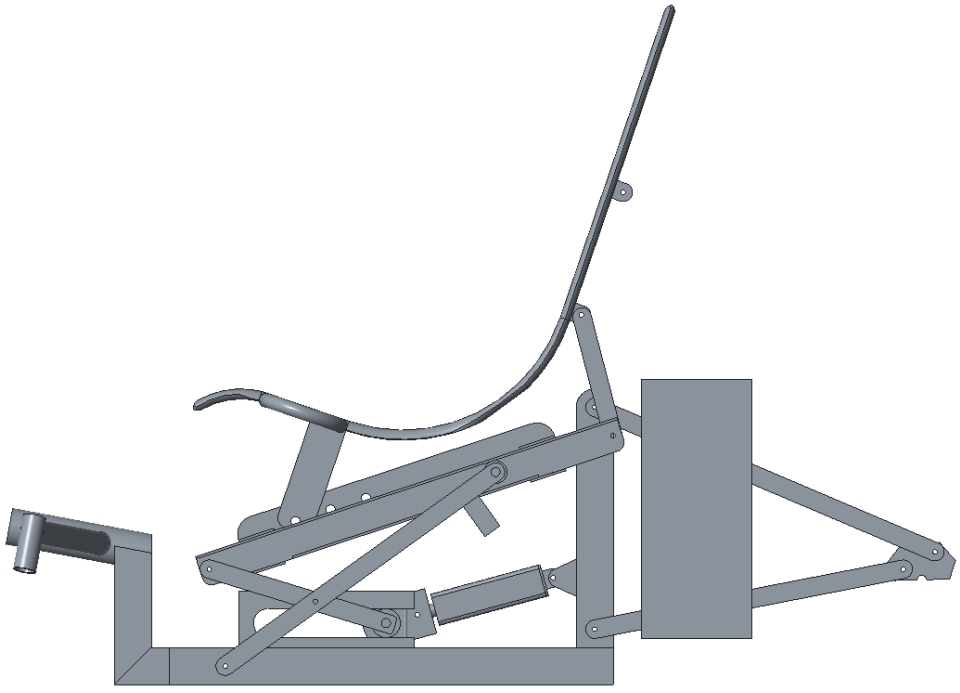

Figure 35: Right-Side View of the Trike in the Lowered Position.

When this model was imported into ANSYS, an initial (default) mesh was generated, as seen in Figure 36.

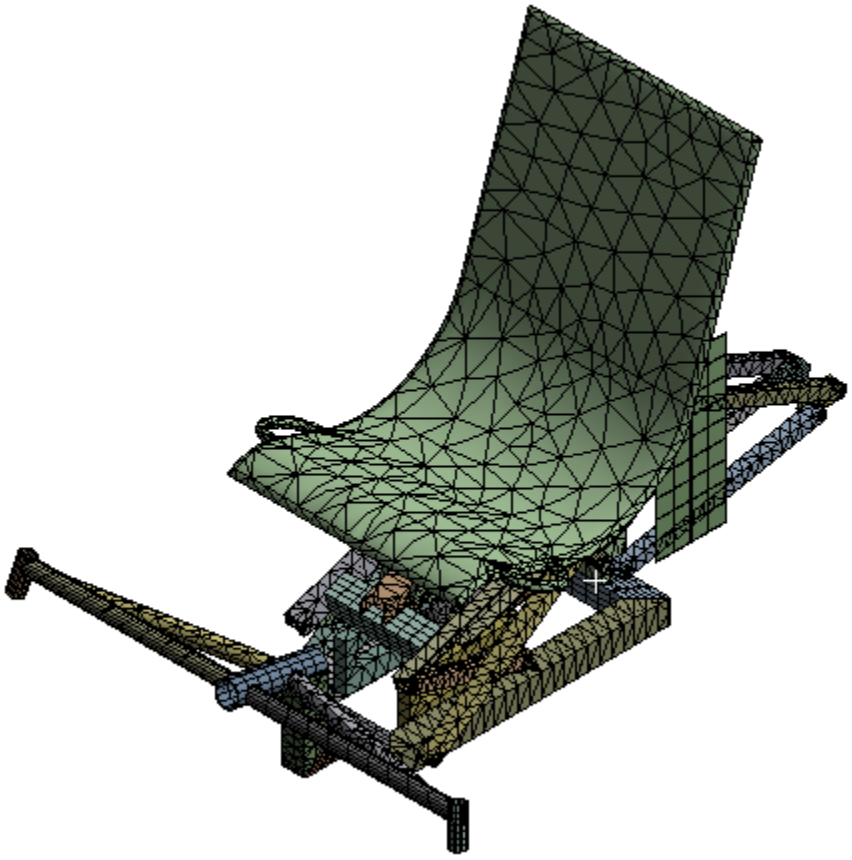

Figure 36: Isometric View of the Frame in the Lowered Position with a Default Mesh.

After the initial mesh was applied to the model, the supports were applied. There were four surfaces selected to be Fixed Supports (the insides of the collars in the front, where the steering tillers are attached to the frame – see Figure 37), and there were two surfaces selected to be Frictionless Supports (the insides of the two rear hubs where the rear wheel is attached to the frame – see Figure 38).

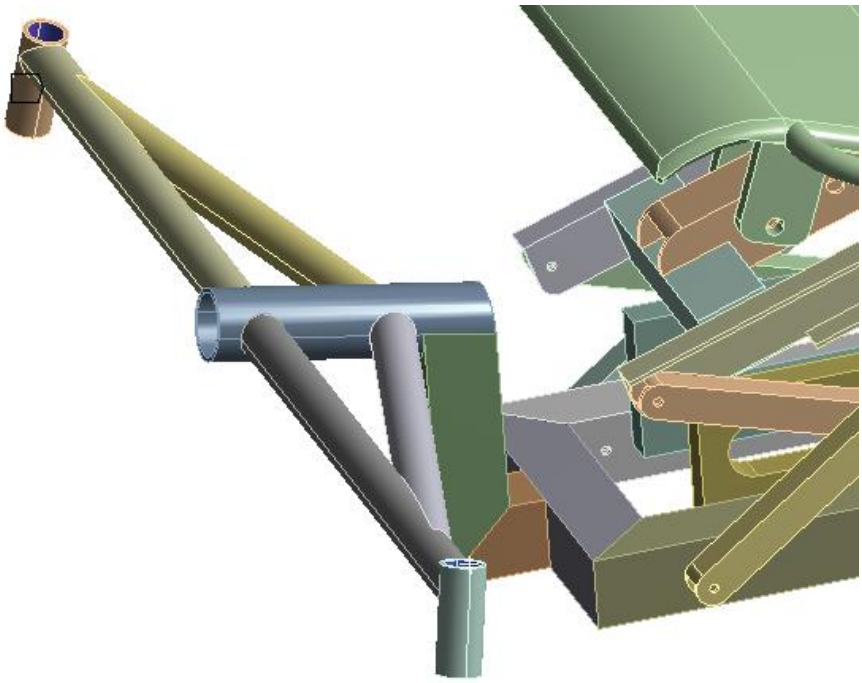

Figure 37: Location of the Fixed Supports for the Lowered Position FEA.

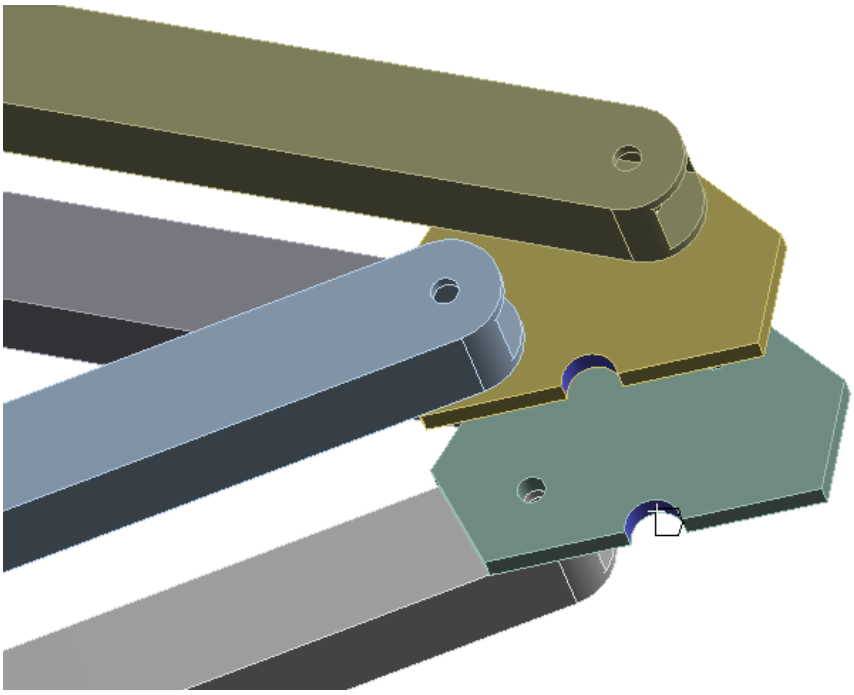

Figure 38: Location of the Frictionless Supports for the Lowered Position FEA.

Next, a Force Load was applied and distributed to the inside surface (four surfaces total) of the seat, as seen in Figure 39.

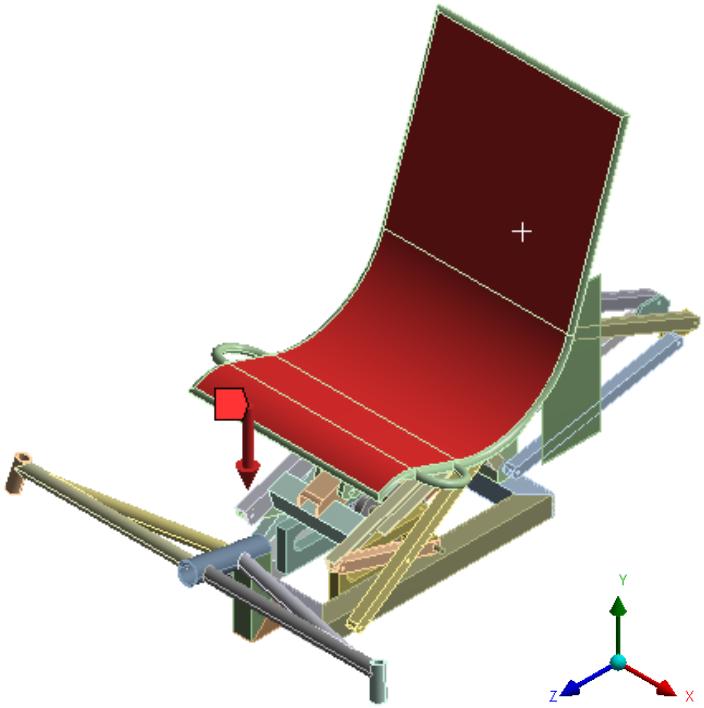

Figure 39: Location of the Applied Force Load, Indicated by the Red Surfaces.

A load of 2670 N was applied in the negative direction of the y-component of this model, which was derived from the previous analysis, based on the maximum recommended load, scaled up by the factor of safety determined by the Pugsley Method. The seat was included in the frame for this reason. It was believed the analysis would be more accurate and true to the real-world application of this trike. If the seat was mounted to the trike and someone sat in it, the highlighted-red surfaces would carry the load of the rider. Although the majority of the weight of the rider would be in the negative direction of the y-component, not all of it would be, as some would be applied backwards in the seat (in the negative direction of the z-component). Since the percentage of load distribution was unknown, it was assumed that the worst case scenario would be when the entire maximum load was applied in one direction (the majority direction). This applied load would then be felt by the rest of the frame, based on the way the frame was designed and assembled.

After the supports and force were applied, the Model Geometry was divided into AISI 1050 and aluminum 6061-T6 groups, where the appropriate materials were applied to the appropriate parts.

Finite Element Analysis of Frame – Raised Position Setup

The other finite element analysis examined the raised position (see Figure 40).

Figure 40: Right-Side View of the Trike in the Raised Position.

When the model was imported into ANSYS, an initial (default) mesh was generated, as seen in Figure 41.

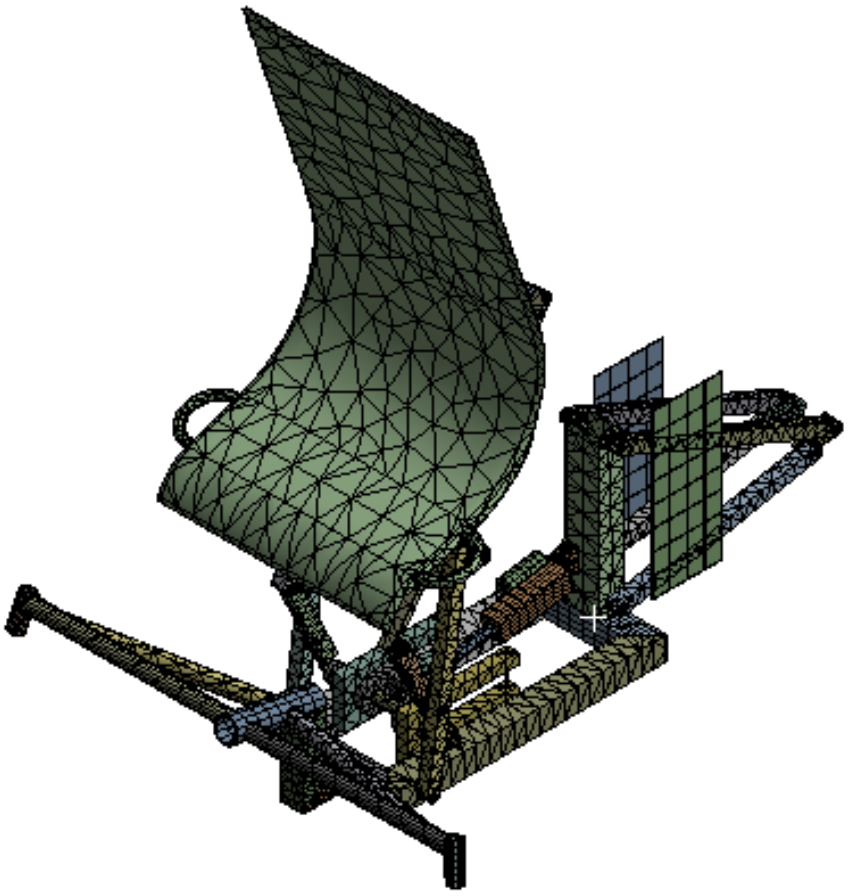

Figure 41: Isometric View of the Frame in the Raised Position with a Default Mesh.

After the initial mesh was applied to the model, the supports were applied. There were four surfaces selected to be Fixed Supports (the insides of the collars in the front, where the steering tillers are attached to the frame – see Figure 42), and there were two surfaces selected to be Frictionless Supports (the insides of the two rear hubs where the rear wheel is attached to the frame – see Figure 43).

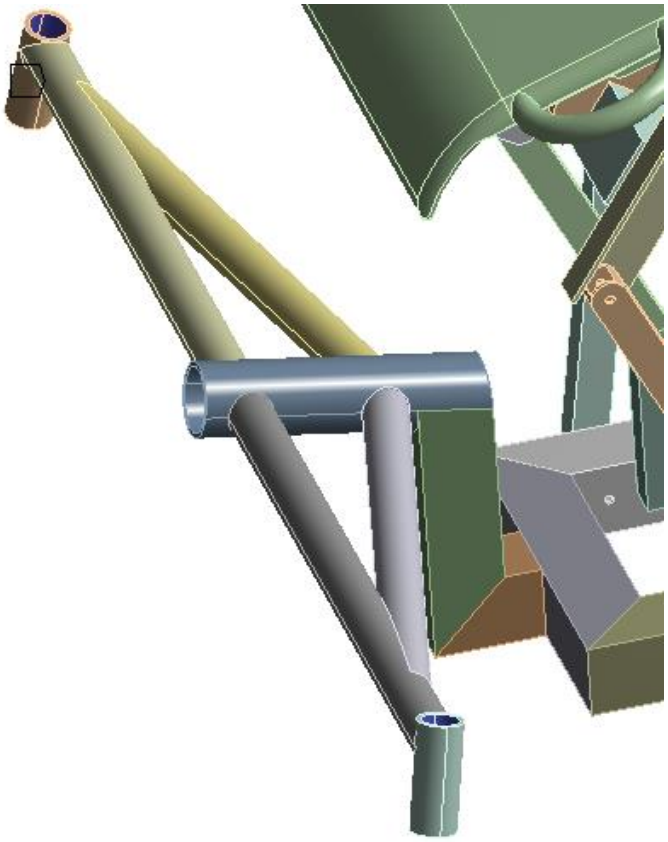

Figure 42: Location of the Fixed Supports for the Raised Position FEA.

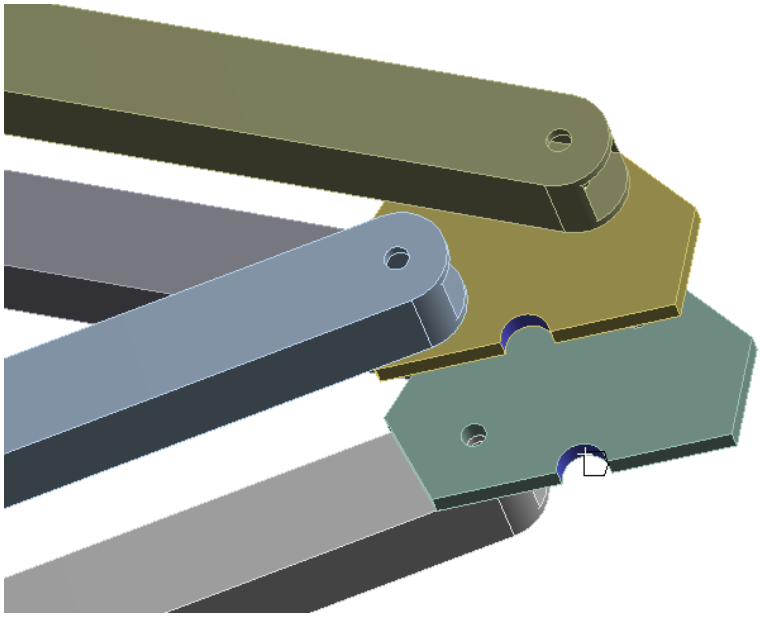

Figure 43: Location of the Frictionless Supports for the Raised Position FEA.

Next, a Force Load was applied and distributed to the inside surface (three surfaces total) of the seat, as seen in Figure 44. This is different than the lowered position FEA, since the topmost surface of the seat was not selected this time.

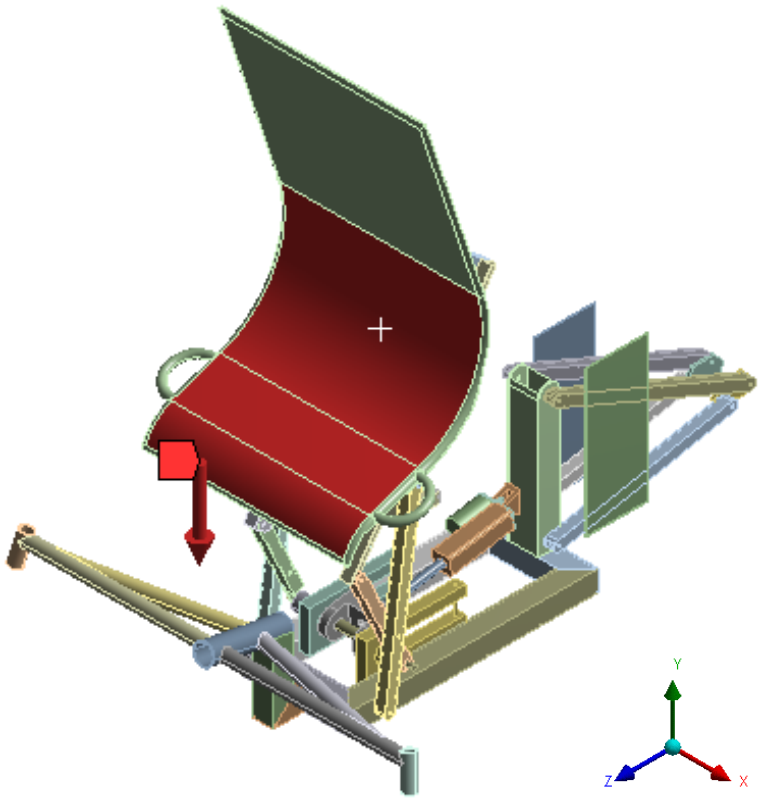

Figure 44: Location of the Applied Force Load, Indicated by the Red Surfaces.

With the seat raised up and the way it is then oriented, it would not make sense for the load to be applied to the topmost surface of the seat, since that part is leaning forward, and when the rider mounts the trike, that part of the seat will hardly be loaded. That being said, a load of 2670 N was applied in the negative direction of the y-component of this model, which was derived from the maximum recommended load, scaled up by the factor of safety determined by the Pugsley Method. The seat was again included in the frame since this part would be the first to carry the load of the rider, which would then distribute the load throughout the rest of the trike based on the

assembly connections. Similar to the previous FEA, there would most likely be a fractional distribution of this load throughout the seat and including the negative direction of the z-component; however, those percentages were not known. Therefore, the worst case scenario was applied; that is, the maximum load was applied purely in the negative direction of the y-component.

After the supports and force were applied, the Model Geometry was divided into AISI 1050 and aluminum 6061-T6 groups, where the appropriate materials were applied to the appropriate parts.

Finite Element Analysis of Frame – Convergence Study

Next, a convergence study was completed for both the raised and lowered positions of the trike. A convergence study can be (and was) used to validate FEA results. For the lowered position, the Solution Methods of Total Deformation, Equivalent (von-Mises) Stress, Maximum Principal Stress, Maximum Shear Stress, and Normal Stress (Y-Axis) were applied to the Model. Since the default mesh was already generated (including an Adaptive Size Function, Coarse Relevance Center, Default Element Size, Medium Smoothing, Fast Transition, and Coarse Span Angle Center), the FEA was solved and the results were recorded. The number of nodes and elements, as well as the mesh statistics, were also recorded.

To complete the convergence study, the mesh Sizing was first changed to a Fine Relevance Center, Slow Transition, and Medium Span Angle Center, whereas the Size Function, Element Size, and Smoothing were left unchanged. Again, the number of nodes and elements and the mesh statistics were recorded, as well as the listed Solution Methods. The sizing characteristics were then left unchanged, whereas the Element Size

was varied and the resulting Solution Methods were recorded. The convergence study was completed by measuring the Total Deformation of one particular node (the same node each time) after varying the Element Size. Convergence was achieved after the Total Deformation approached a horizontal asymptote – that is, where the deformation was irrespective of the element size. Once the asymptote was achieved, a few points past its start was chosen to be the Element Size used to record FEA results. These two points were chosen, as opposed to the last Element Size (the smallest), because this would yield similar results as more nodes (smaller elements), but would require less computing time to solve the FEA. The Total Deformation of one particular node versus the number of nodes was plotted for both the lowered and raised positions, and shown in Figure 45 and Figure 46, respectively.

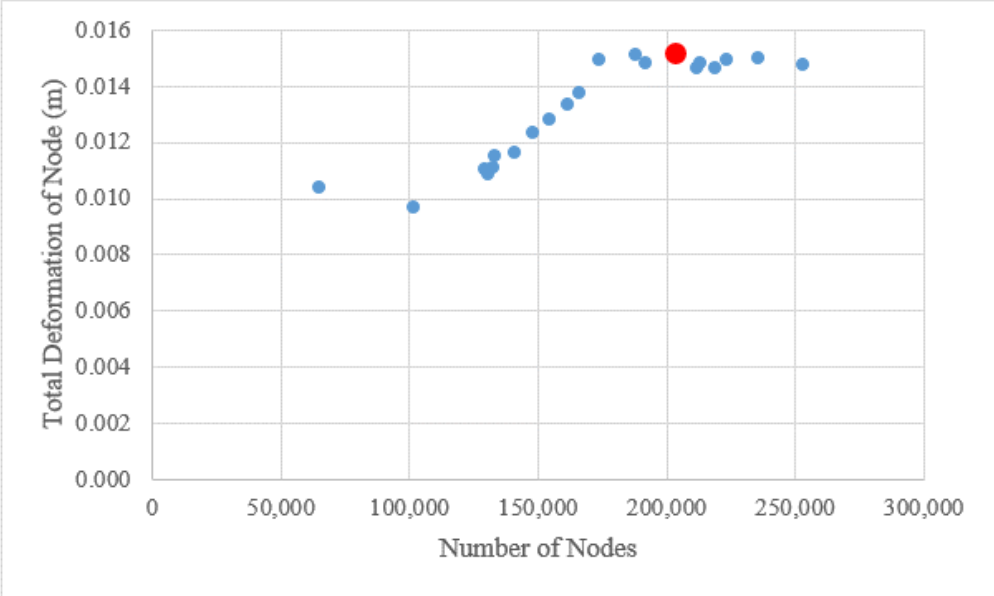

Figure 45: Convergence Study for Lowered Position.

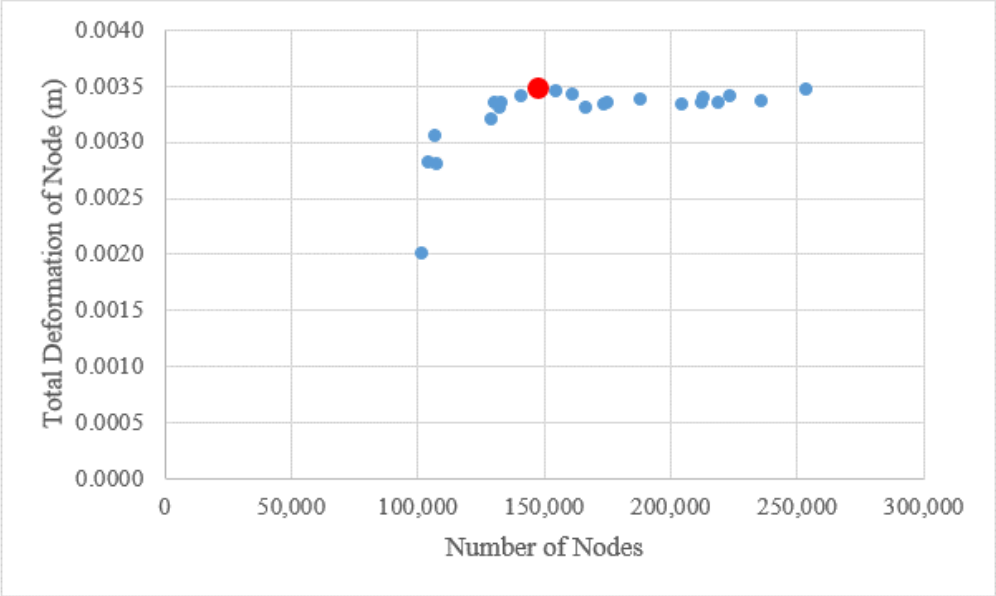

Figure 46: Convergence Study for Raised Position.

The plotted convergence studies show the horizontal asymptote that appears for the Total Deformation as the number of nodes increases. As can be seen in both plots, the larger, red data points represent the chosen nodes and Element Sizes, which appear to be a few points in from the start of the asymptotes.

This convergence study methodology was completed for the lowered and raised positions of the trike. For the lowered position, the mesh had an Adaptive Size Function, Fine Relevance Center, Medium Smoothing, Slow Transition, and Medium Span Angle Center. The large, red data point in Figure 45 corresponds to a 29 mm maximum Element Size, which resulted in a mesh of 204,363 nodes and 110,589 elements. For the raised position, the mesh parameters were the same as the lowered position; however, the large, red data point in Figure 46 corresponds to a 50 mm maximum Element Size, which resulted in a mesh of 148,143 nodes and 83,898 elements. These two specific cases were chosen to be the Element Sizes for their respective (lowered or raised) positions.

To validate the quality of the mesh, a Skewness Mesh Metric was tracked for each iteration throughout the convergence studies. In reference to the angles of the cells, the "skewness determines how close to ideal (that is, equilateral or equiangular) a face or cell is" [39]. The ranges and cell quality of calculated skewness can be found in Table 7, which was used in determining the quality of the meshing in this project.

Table 7: Skewness Ranges and Corresponding Cell Qualities [39].

Skewness	Cell Quality
1	degenerate
0.9 – <1	bad (sliver)
0.75 – 0.9	poor
0.5 – 0.75	fair
0.25 – 0.5	good
>0 – 0.25	excellent
0	equilateral

For the chosen Element Size for the lowered position, the Skewness Mesh Metric average was 0.57178 with a standard deviation of 0.26215, whereas the Skewness Mesh Metric average was 0.58148 with a standard deviation of 0.29115 for the chosen Element Size for the raised position. Referring to Table 7, the lowered and raised positions had fair cell quality, but with the standard deviations, the cell quality was good in some areas (as well as poor). Improving the mesh of each individual part of the model could improve the quality of the mesh, which could improve the mesh statistics and cell qualities.

Finite Element Analysis of Frame – Results

The results of the listed Solution Methods were recorded for the chosen Element Sizes. Again, these two Element Sizes were chosen after completing convergence studies, which were validated by Skewness Mesh Metrics (which were not perfect, but valid nonetheless). Summarized in Table 8 are the mesh details and solutions to the lowered and raised positions.

Table 8: Summarized Mesh Details and FEA Solutions for Both Positions.

Parameter	Position	
	Lowered	Raised
Size Function	Adaptive	Adaptive
Relevance Center	Fine	Fine
Element Size (mm)	29	50
Smoothing	Medium	Medium
Transition	Slow	Slow
Span Angle Center	Medium	Medium
Nodes (#)	204,363	148,143
Elements (#)	110,589	83,898
Mesh Metric Min	0.01668	0.00404
Mesh Metric Max	0.99997	0.99979
Mesh Metric Average	0.56439	0.55089
Mesh Metric StdDev	0.22035	0.25890
Total Deformation (mm)	16	4
Equivalent (von-Mises) Stress (MPa)	272	222
Maximum Principal Stress (MPa)	266	276
Maximum Shear Stress (MPa)	156	126
Normal Stress, Y-Axis (MPa)	134	80

The following figures (Figure 47, Figure 48, and Figure 49) show some Solution Methods for the lowered position.

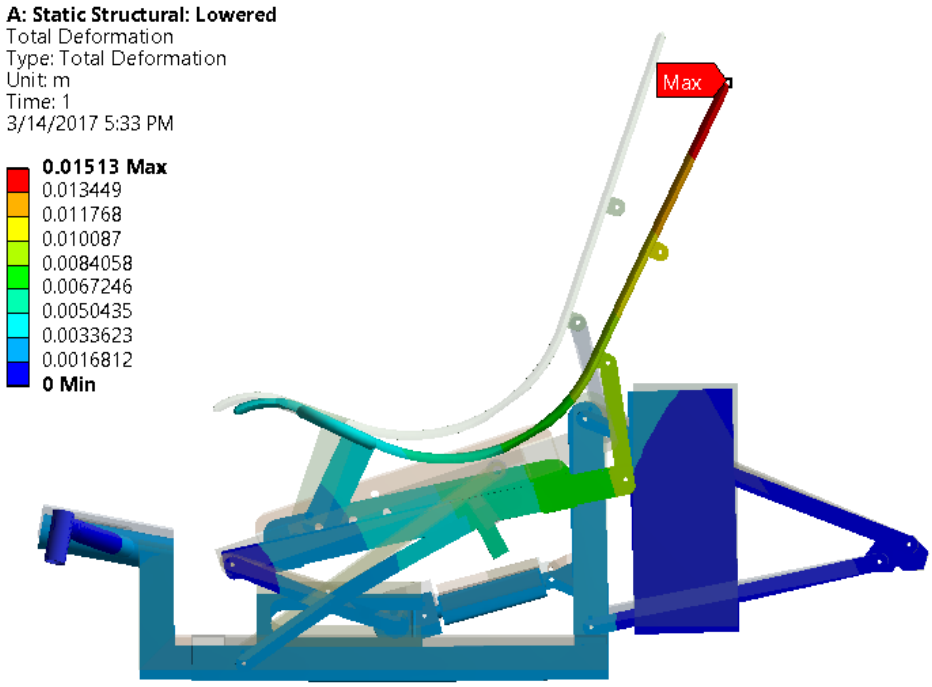

Figure 47: Total Deformation, with Undeformed Model Showing (7.9x Scale).

Figure 47 shows the Total Deformation with the undeformed model and a 7.9x scale to display how the frame would deform under the load, whereas Figure 48 shows the Total Deformation with the undeformed model and a true (1x) scale to display how the frame actually deforms under the load. No interferences resulted from this deformation (maximum of less than 16 mm occurring at the top of the seat), so there are no concerns with this portion of the results.

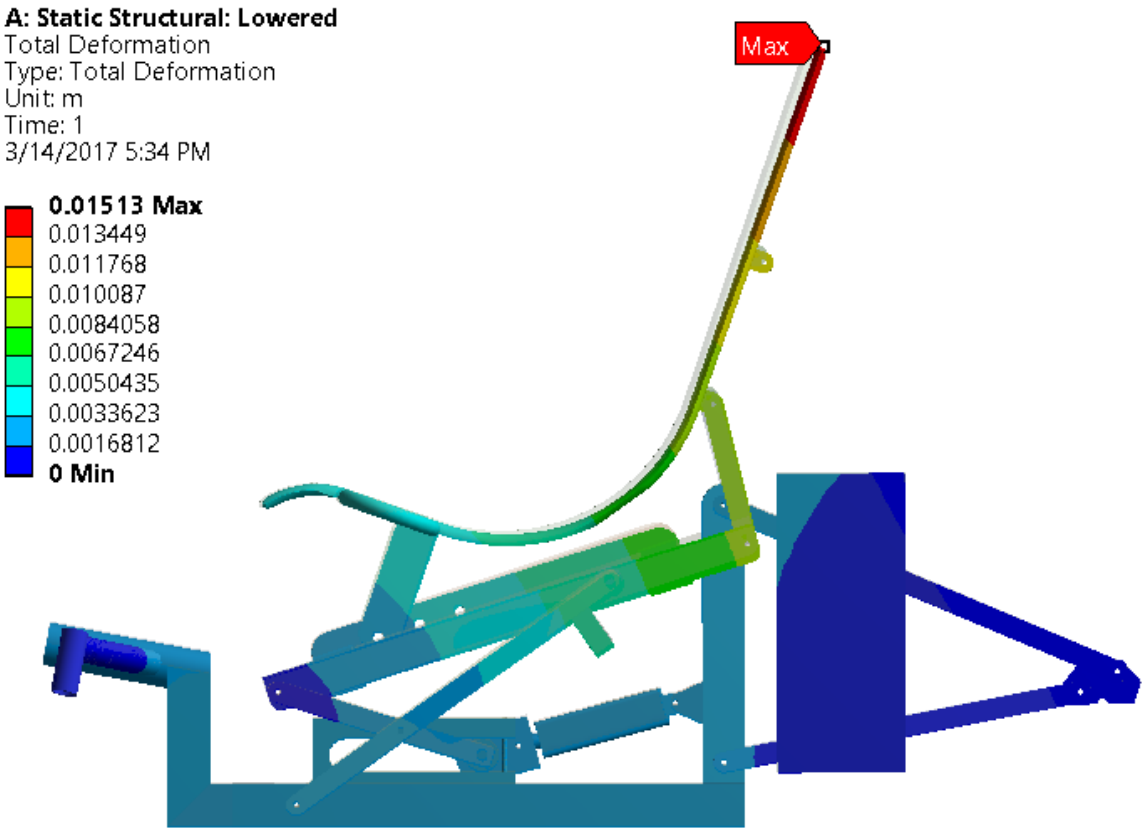

Figure 48: Total Deformation, with Undeformed Model Showing (True Scale).

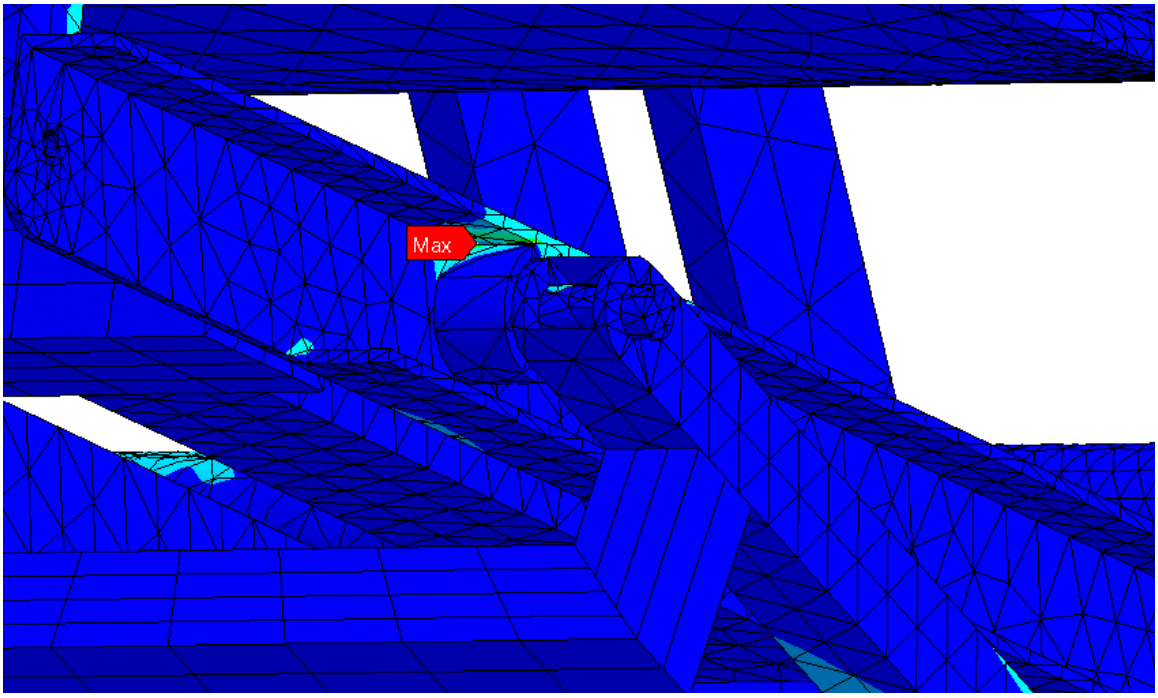

Figure 49: Equivalent (von-Mises) Stress, Showing Maximum Stress Location.

The maximum Equivalent (von-Mises) Stress experienced in the lowered position occurs where the right roller meets the right channel, as shown in Figure 49. The roller is made from steel and the channel is made from aluminum. The FEA calculated the maximum stress has a magnitude of approximately 272 MPa, which is below the yield strengths of aluminum 6061-T6 (276 MPa) and AISI 1050 (515 MPa), so this design should not fail under the maximum load. The same conclusion applies throughout the rest of the design and Solution Methods, as the Maximum Principal, Maximum Shear, and Normal Stresses are all less than the Equivalent Stress. There are some negative forces (compression) experienced in some areas of this trike, but the magnitudes of these compressive forces are less than those of the positive forces (tension). Therefore, if a part of this trike were to fail, that part would probably fail in tension.

The following figures (Figure 50, Figure 51, and Figure 52) show some Solution Methods for the raised position.

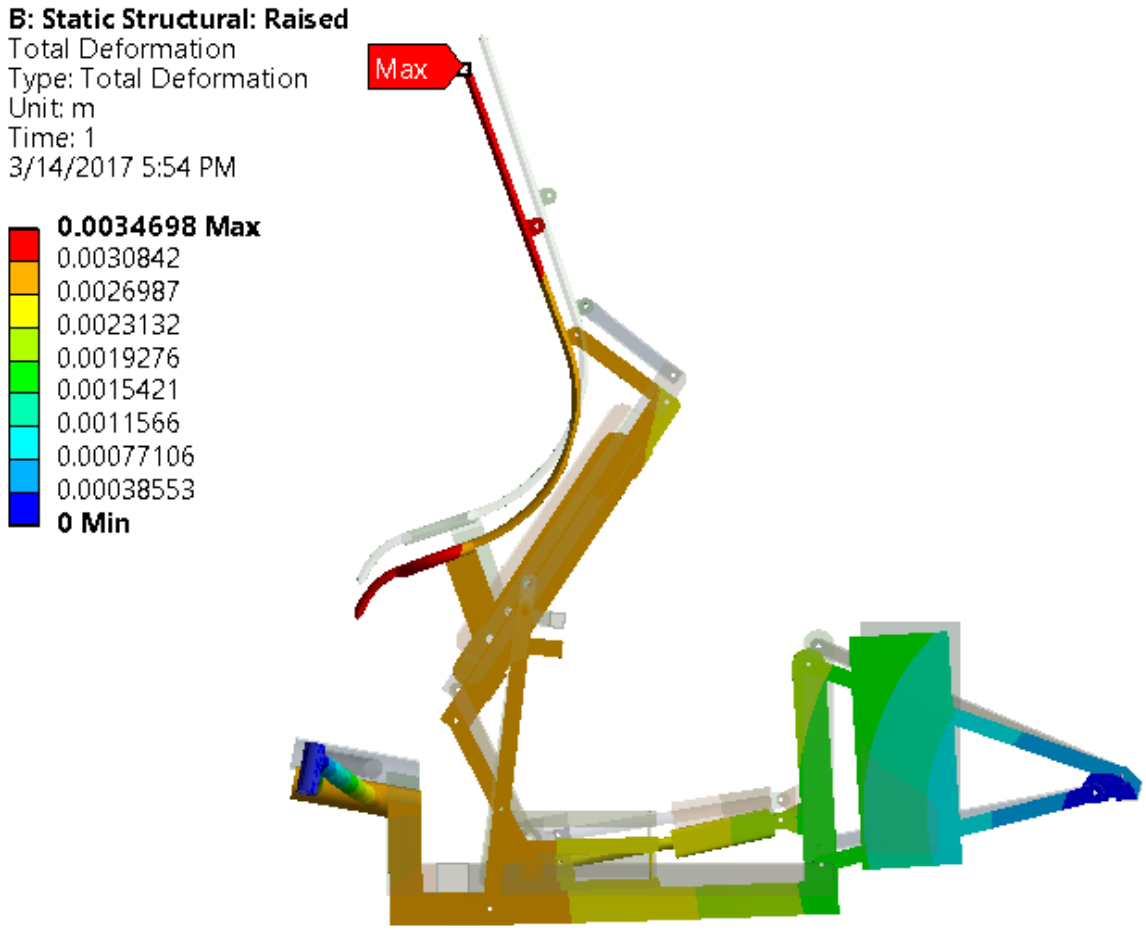

Figure 50: Total Deformation, with Undeformed Model Showing (16x Scale).

Figure 50 shows the Total Deformation with the undeformed model and a 16x scale to display how the frame would deform under the load, whereas Figure 51 shows the Total Deformation with the undeformed model and a true (1x) scale to display how the frame actually deforms under the load. No interferences resulted from this deformation (maximum of less than 4 mm occurring at the top of the seat), so there are no concerns with this portion of the results.

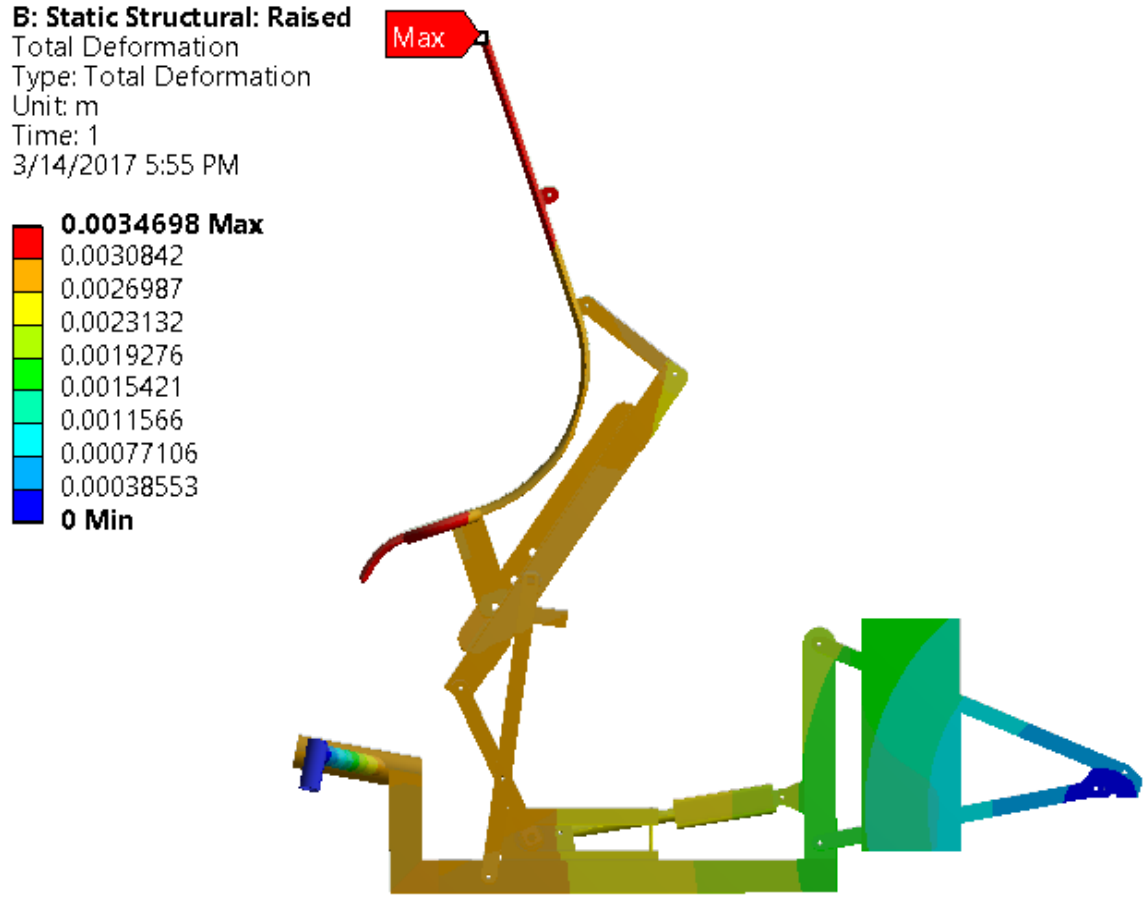

Figure 51: Total Deformation, with Undeformed Model Showing (True Scale).

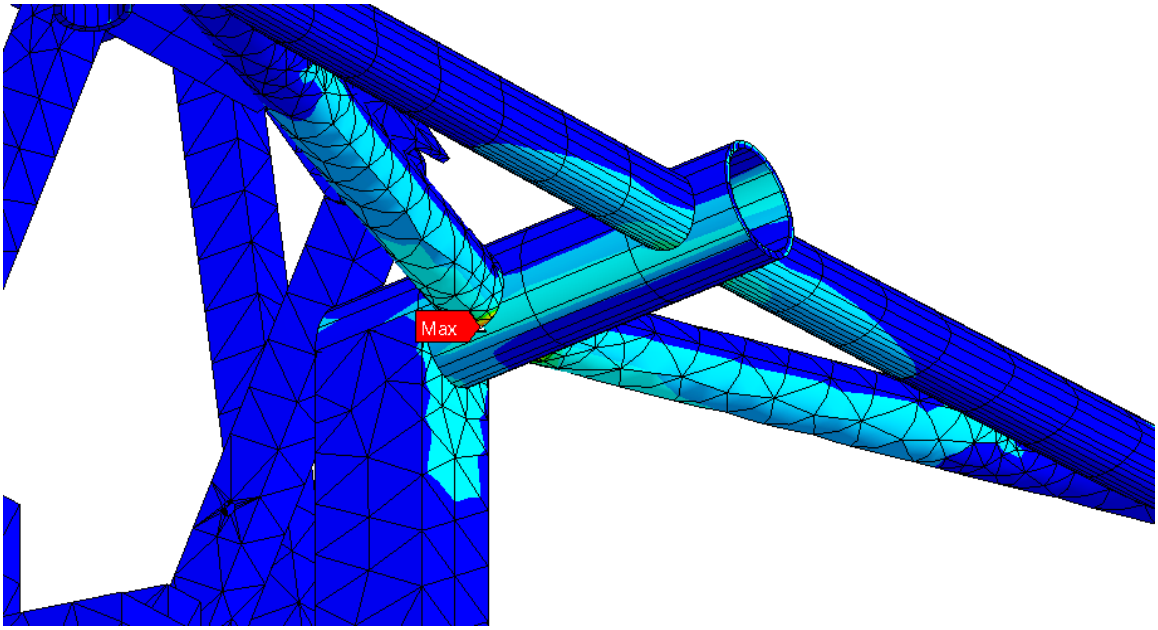

Figure 52: Maximum Principal Stress, Showing Maximum Stress Location.

The Maximum Principal Stress experienced in the lowered raised position occurs where a boom support gusset tube meets the boom housing tube, as shown in Figure 52. Both of these tubes are made from aluminum 6061-T6. The FEA calculated the maximum stress has a magnitude of just under 276 MPa, which is approximately the yield strength of aluminum 6061-T6 (276 MPa). That being said, if this design were to fail, it would probably fail in tension. There are some negative forces (compression) experienced in some areas of this trike, however, but the magnitudes of these compressive forces are less than those of the positive forces (tension), as calculated by the Equivalent (von-Mises) Stress, Maximum Shear Stress, and Normal Stress Solution Methods. Nevertheless, the maximum stress is slightly less than the material yield strength, so the design should not fail under the maximum load.

Finite Element Analysis of Frame – Summary

Early trials of the lowered and raised positions of the trike were analyzed in ANSYS, which included the racks for the gears' rack and pinion systems. However, the reason the racks were removed from the frame assembly is because the maximum equivalent stresses were occurring at the locations the gears met the gear racks. When the mesh was refined around these maximum stress areas, the maximum equivalent stresses increased for both scenarios. It was concluded from this that the meshing and refinement methods were not successful. As a result, the gear stress analyses were completed separately (in MATLAB – details on results above and code provided in Appendix B), and the gears and racks were removed from the trike frame assembly (the gears were replaced by geometrically similar cylinders).

Once the gear racks were removed and the gears were replaced, FEA was completed on the two positions. First, a convergence study and mesh analysis was completed for validity of the FEA, and the results were recorded and detailed above.

Overall, the FEA of the lowered and the raised positions of the trike represent the minimum and maximum positions the trike can be oriented. The results (maximum equivalent stress and maximum total deformation) proved the frame design is safe in both of these positions – the lowered and raised. Therefore, since the minimum and maximum positions were determined to be safe (via gear stress analysis and FEA), the design was determined to be safe for all positions in between – this is provided that the velocity of position change is slow, which it is. The FEA proved the frame design is safe in all positions of the seat since the minimum and maximum positions were analyzed (and survived) under the worst case of the maximum recommended load.

CONCLUSIONS AND RECOMMENDATIONS

In this project, the design and analysis of a human powered vehicle (trike) was completed. There was an original design and prototype of a trike called the Heliocycle, which was the foundation for this project. After the original Heliocycle reached various parts of the public, feedback was gathered regarding how it could be improved. Focusing on only a few suggestions, this project entailed the redesign of the Heliocycle, followed by the analysis of this redesign. The CAD modeling was completed in PTC Creo Parametric 2.0/3.0, whereas the engineering analysis was completed in MATLAB R2015b and ANSYS 17.2. The redesign included completely original CAD renderings, and the engineering analysis included the determination of the design factor of safety, gear stress analysis, and finite element analysis. The engineering analysis proved that the design was safe and could withstand the maximum recommended load of 300 lb_m.

If this project was to be redone or continued, several facets could be improved or explored. First, the rack and pinion system that was chosen for the redesign included spur gears, but other types of gears could be tried. Also, different materials (e.g., different alloys or carbon fiber) could be implemented for the frame's composition. Another way the results can be made more realistic is if authentic CAD files for off-the-shelf parts from vendors are incorporated into the trike assembly, which may improve the accuracy of the analysis. Moreover, early FEA included the rack and pinion systems on the frame, but it was determined this analysis was unsuccessful. If this was explored more, results may have improved. Regardless, the AGMA calculations via *Shigley's Mechanical Engineering Design* book and formulas are solid analytical tools that should be used.

FEA results could have been further improved if each model member was individually meshed. Improving the mesh of the model could have improved the end results and calculated solutions. Also, the mesh cell quality could have been improved by improving the mesh, which would result in greater validity and accuracy of the results.

REFERENCES

[1] B. Chu, "Recumbent Bikes vs. Trikes," WordPress.com, 15 February 2011. [Online]. Available: https://proporzionedivina.wordpress.com/2011/02/15/recumbent-bikes-vs-trikes/. [Accessed 7 November 2016].

[2] ActionBent, "ActionBent T1X Suspended Tadpole Trike," WordPress.com, [Online]. Available: https://trikeasylum.wordpress.com/company-information/specs-a-m/actionbent/. [Accessed 7 November 2016].

[3] H. Thomas, "Tadpole or Delta," Jetrike, 9 November 2007. [Online]. Available: http://www.jetrike.com/tadpole-or-delta.html. [Accessed 7 November 2016].

[4] Machine Design Staff, "Unchained Innovation," Machine Design, 6 October 2005. [Online]. Available: http://machinedesign.com/news/unchained-innovation. [Accessed 7 November 2016].

[5] J. X. Weinert, A. F. Burke and X. Wei, "Lead-acid and Lithium-ion Batteries for the Chinese Electric Bike Market and Implications on Future Technology Advancement," ScienceDirect - Journal of Power Sources, 25 October 2007. [Online]. Available: http://www.sciencedirect.com/science/article/pii/S0378775307010294. [Accessed 7 November 2016].

[6] J. Forester, "Effective Cycling," MIT Press, 1 April 2012. [Online]. Available: http://ezproxy.msoe.edu:2129/xpl/bkabstractplus.jsp?reload=true&bkn=6267545. [Accessed 7 November 2016].

[7] D. Bustamante, "Road Bike Disc Brakes – A Clear Case Of The 'No-Brainer'," Tweaked Sports, 17 October 2012. [Online]. Available: http://cyclingdynamics.blogspot.com/2012/10/road-bike-disc-brakes-clear-case-of-no.html. [Accessed 7 November 2016].

[8] S. Brown, "Adjusting Direct-pull Cantilever Bicycle Brakes," Harris Cyclery, 2008. [Online]. Available: http://sheldonbrown.com/canti-direct.html. [Accessed 7 November 2016].

[9] B. S. Helm, K. G. Bauserman, M. J. Caelwaerts and N. W. Weis, "Vehicle with Seat Lift System". United States of America Patent 62/392,107, 20 May 2016.

[10] I. Peters, "IBISWorld Industry Report OD4357," IBISWorld , September 2016. [Online]. Available: http://ezproxy.msoe.edu:2536/reports/us/industry/ataglance.aspx?entid=4357. [Accessed 17 February 2017].

[11] W. Sloan, "Bicycle Fitting Apparatus and Method". United States of America Patent US8544947 B2, 1 October 2013.

[12] P. Steller, "Electric Tricycle". United States of America Patent US3598195 A, 10 August 1971.

[13] C. L. Prince, "Rear Wheel Suspension System for a Tricycle Vehicle". United States of America Patent US4887829 A, 19 December 1989.

[14] Wikimedia Foundation, Inc., "Finite Element Method," Wikipedia, 2016. [Online]. Available: https://en.wikipedia.org/wiki/Finite_element_method. [Accessed 8 November 2016].

[15] V. Gulati, S. Mehta, A. Kashyap and K. Pawar, "Design and FEA of a Recumbent Trike," *International Journal of Applied Engineering Research,* vol. 7, no. 11, 2012.

[16] M. Gföhler, M. Loicht and P. Lugner, "Exercise Tricycle for Paraplegics," *Medical & Biological Engineering & Computing,* pp. 118-121, 1998.

[17] V. P and R. R, "Design and Concept Evaluation of Tricycle for Aged and Orthopedic Differentially Abled Persons," *International Journal of Computer Applications,* vol. 111, no. 15, pp. 18-25, February 2015.

[18] R. B. Cunha, G. G. Mendes Marra, P. P. Brito and C. B. Santos Vimieiro, "Development of an Adaptive KIT for Wheelchair Turning it into an Electric Tricycle," *Applied Mechanics and Materials,* vol. 775, pp. 98-102, 2015.

[19] T. I. Kosmanis and T. V. Yioultsis, "Electrical Drivetrains for Tad-pole and Delta Type Recumbent Tricycles," *International Conference on Connected Vehicles and Expo (ICCVE),* 2014.

[20] L. Blaga, "Analysis Based Optimization of Human Powered Vehicle Body," *Applied Mechanics and Materials,* vol. 760, pp. 123-128, 18 May 2015.

[21] R. G. Budynas and J. K. Nisbett, *Shigley's Mechanical Engineering Design*, 10th ed., New York, New York: McGraw-Hill Education, 2015, pp. 665-776.

[22] Seaten Industry & Trade Co. Ltd., "Electric Car Jack, Used for SUV," Media Data Systems Pte Ltd, 2016. [Online]. Available: http://www.globalsources.com/si/AS/Seaten-Industry/6008830797885/pdtl/Electric-car-jack/1064644061.htm. [Accessed 8 November 2016].

[23] Joyce Dayton, "50 Ton Machine Screw Jacks (WJT1150, WJT3250)," Joyce Dayton, 2013. [Online]. Available: http://joycedayton.com/products/machine-screw-jacks/50-ton-machine-screw-jacks. [Accessed 8 November 2016].

[24] Parker Hannifin Corp, "Hydraulic Rotary Actuator - Tork-Mor Series (Vane)," Parker Hannifin, 2015. [Online]. Available: http://ph.parker.com/us/en/hydraulic-rotary-actuator-tork-mor-series-vane. [Accessed 8 November 2016].

[25] B. Bartos, "Strengths & Limitations: Belt Drive vs. Ball Screw Actuators," MISUMI Corporation, 20 March 2015. [Online]. Available: http://blog.misumiusa.com/strengths-limitations-belt-drive-vs-ball-screw-actuators/. [Accessed 8 November 2016].

[26] MotoAlliance, "VIPER Winch Replacement Parts (Classic 2500/3000/3500/4000)," MotoAlliance, 2016. [Online]. Available: https://motoalliance.com/Site.ReplacementParts.ViperATVUTVWinches.Classic2500300035004000.go. [Accessed 8 November 2016].

[27] Berkeley Science Books, "Synopsis of Mathematical Modeling and Computational Calculus I - Calculus Without Tears," Berkeley Science Books, [Online]. Available: http://berkeleyscience.com/MMCCI.htm. [Accessed 8 November 2016].

[28] Firgelli Automations, "Feedback Rod Linear Actuators," Firgelli Automations, 2016. [Online]. Available: https://www.firgelliauto.com/products/feedback-rod-actuator. [Accessed 8 November 2016].

[29] A. Hornbacher, "Steel versus Aluminum: Weight, Strength, Cost, Malleability Comparison," Wenzel Metal Spinning, 2017. [Online]. Available: http://www.wenzelmetalspinning.com/steel-vs-aluminum.html. [Accessed 14 March 2017].

[30] Progressive Automation, Inc., "PA-03-6-600 Linear Actuator," Progressive Automation, Inc., 2017. [Online]. Available: https://www.progressiveautomations.com/linear-actuator. [Accessed 17 February 2017].

[31] D. O. Anderson, Ph.D., "Safety Factor," Louisiana Tech University, 2001. [Online]. Available: http://content.lms.sabis.sakarya.edu.tr/Uploads/49092/29725/safety_factor.pdf. [Accessed 17 February 2017].

[32] J. Koerlin, "Pound-force (lbf) vs Pound-mass (lbm)," Stack Exchange, Inc., 25 August 2015. [Online]. Available: http://engineering.stackexchange.com/questions/2300/pound-force-lbf-vs-pound-mass-lbm. [Accessed 17 February 2017].

[33] McMaster-Carr Supply Company, "High-Load Metal Gear - 20 Degree Pressure Angle," McMaster-Carr Supply Company, 2015. [Online]. Available: https://www.mcmaster.com/#5172T42. [Accessed 17 February 2017].

[34] MyTimeMedia Ltd, "Which Grade of Steel Required to Make Gears," MyTimeMedia Ltd, 14 June 2010. [Online]. Available: http://www.model-engineer.co.uk/forums/postings.asp?th=40868. [Accessed 17 February 2017].

[35] Wikimedia Foundation, Inc., "Carbon Steel," Wikimedia Foundation, Inc., 3 January 2017. [Online]. Available: https://simple.wikipedia.org/wiki/Carbon_steel. [Accessed 17 February 2017].

[36] eFunda, Inc., "Medium-Carbon Steels," eFunda, Inc., 2017. [Online]. Available: http://www.efunda.com/materials/alloys/carbon_steels/medium_carbon.cfm. [Accessed 17 February 2017].

[37] MatWeb, LLC, "AISI 1050 Steel, as Cold Drawn Bar, 50-75 mm (2-3 in) Round," MatWeb, LLC, 2017. [Online]. Available: http://www.matweb.com/search/DataSheet.aspx?MatGUID=9b8279fc95c043368b0d1b8589fc0cda&ckck=1. [Accessed 17 February 2017].

[38] MatWeb, LLC, "Aluminum 6061-T6; 6061-T651," MatWeb, LLC, 2017. [Online]. Available: http://www.matweb.com/search/DataSheet.aspx?MatGUID=b8d536e0b9b54bd7b69e4124d8f1d20a. [Accessed 17 February 2017].

[39] SAS IP, Inc., "21.2.4. Quality Measure," SAS IP, Inc., 2017. [Online]. Available: https://www.sharcnet.ca/Software/Ansys/17.0/en-us/help/tgd_usr/tgd_user_report_qualitymeasure.html. [Accessed 14 March 2017].

APPENDIX A: CODES AND STANDARDS DESCRIPTIONS

ASTM F2711-08 (2012) Standard Test Methods for Bicycle Frames

"5.1 These tests are used to verify the durability and strength of a bicycle frame.

1. Scope

1.1 These test methods establish procedures for conducting tests to determine the structural performance properties of bicycle frames.

1.2 These test methods describe mechanical tests for determining the following performance properties:

1.2.1 Frame Fatigue—Horizontal Loading,

1.2.2 Frame Fatigue—Vertical Loading, and

1.2.3 Frame Impact Strength.

1.3 The values stated in SI units are to be regarded as standard. No other units of measurement are included in this standard.

1.4 This standard does not purport to address all of the safety concerns, if any, associated with its use. It is the responsibility of the user of this standard to establish appropriate safety and health practices and determine the applicability of regulatory limitations prior to use."

ISO 1143:1994 Cycles – Luggage Carriers for bicycles – Concepts, classification and testing

"Specifies dimensions and performance requirements for luggage carriers intended for mounting above the rear wheels of bicycles."

ISO 4210-1:2014 Cycles – Safety Requirements for Bicycles

"ISO 4210-1:2014 specifies terms and definitions related to safety and performance requirements for the design, assembly, and testing of bicycles and sub-assemblies having saddle height as given in Table 1.

ISO 4210-2:2014 specifies safety and performance requirements for the design, assembly, and testing of bicycles and sub-assemblies having saddle height as given in Table 1, and lays down guidelines for manufacturer's instructions on the use and care of such bicycles.

ISO 4210-3:2014 specifies the common test methods for ISO 4210 2. ISO 4210-4:2014 specifies the braking test methods for ISO 4210 2. ISO 4210-5:2014 specifies the steering test methods for ISO 4210 2. ISO 4210-6:2014 specifies the frame and fork test methods for ISO 4210 2. ISO 4210-7:2014 specifies wheel and rim test methods for ISO 4210 2. ISO 4210-8:2014 specifies pedal and drive system test methods for ISO 4210 2. ISO 4210-9:2014 specifies saddle and seat-post test methods for ISO 4210 2."

ISO 6698:1989 Cycles – Screw threads used to assemble freewheels on bicycle hubs

"Specifies the thread profile and limits and tolerances for the screw threads used to assemble freewheels on bicycle hubs. Based on the use of the ISO basic thread profile, satisfactory interchangeability with the corresponding B.S.C. thread, the use of screw thread tolerance grades and tolerance positions and the use of gauges made to ISO 1502."

ISO 8098:2014 Cycles – safety requirements for bicycles for young children

> "ISO 8098:2014 specifies safety and performance requirements and test methods for the design, assembly and testing of fully assembled bicycles and sub-assemblies for young children. It also provides guidelines for instructions on the use and care of the bicycles."

ISO 12405-1:2011 Electrically propelled road vehicles – Test specification for lithium-ion traction battery packs and systems – Part 1: High-power applications

> "ISO 12405-1:2011 specifies test procedures for lithium-ion battery packs and systems for use in electrically propelled road vehicles. The specified test procedures enable the determination of the essential characteristics of performance, reliability and abuse of lithium-ion battery packs and systems. They assist the user of ISO 12405-1:2011 to compare the test results achieved for different battery packs or systems. Therefore, ISO 12405-1:2011 specifies standard test procedures for basic characteristics of performance, reliability and abuse of lithium-ion battery packs and systems. It enables the setting up of a dedicated test plan for an individual battery pack or system subject to agreement between the customer and supplier. If required, the relevant test procedures and/or test conditions of lithium-ion battery packs and systems can be selected from the standard tests provided in ISO 12405-1:2011 to configure a dedicated test plan. ISO 12405-1:2011 specifies tests for high-power battery packs and systems."

ISO 12405-3:2014 Electrically propelled road vehicles – Test specification for lithium-ion traction battery packs and systems – Part 3: Safety performance requirements

> "ISO 12405-3:2014 specifies test procedures and provides acceptable safety requirements for voltage class B lithium-ion battery packs and systems, to be used as traction batteries in electrically propelled road vehicles. Traction battery packs and systems used for two-wheel or three-wheel vehicles are not covered by ISO 12405-3:2014. ISO 12405-3:2014 is related to the testing of safety performance of battery packs and systems for their intended use in a vehicle. ISO 12405-3:2014 is not intended to be applied for the evaluation of the safety of battery packs and systems during transport, storage, vehicle production, repair, and maintenance services."

ISO/DIS 6742 Cycles – Lighting and retro-reflective devices – Parts 1, 2, 3, 5.

For more information on ISO/DIS 6742 (Parts 1, 2, 3, 5), see the ISO website.

1. Lighting and light signaling devices
2. Retro-reflective devices
3. Installation and use of lighting and retro-reflective devices
5. Lighting systems not powered by the cycle's movement

ISO/TR 10687:2012 Mechanical vibration – Description and determination of seated postures with reference to whole-body vibration

> "ISO/TR 10687:2012 summarizes descriptive quantities for those responsible (e.g. scientists, safety engineers) for determination of postures for a seated person who is exposed to whole-body vibration. It is the intention that the results of different methods which also are summarized can be easily related to these quantities and that they allow for a common terminology between practitioners. The postures determined can also be used as a basis for further investigation or as a means of comparison for different methods. Although some of the approaches described here can be applied to standing or recumbent positions, additional considerations are likely to be required in these cases. Additionally, ISO/TR 10687:2012 deals with dynamic postures where body angles or associated movements are determined visually or by measuring points on the skin or clothing. ISO/TR 10687:2012 does not recommend sampling strategies or evaluation methods."

APPENDIX B: MATLAB CODE FOR GEAR STRESS ANALYSIS

```
%% Capstone - Gear Stress Analysis
% Bradley Helm
% Dr. Subha K. Kumpaty, Dr. Nebojsa Sebastijanovic, Professor Gary Shimek
% GE-798/101
% 2017-02-10
clear; clc; close all

%% Factor of Safety Determination
% Calculate the factor of safety using the Pugsley Method.
% http://content.lms.sabis.sakarya.edu.tr/Uploads/49092/29725/safety_factor.pdf
% N=N1*N2 where N is the factor of safety and N1=f(A,B,C) and N2=f(D,E)
% A=VG, C=G, B=G, D=S, E=S
N1 = 1.45; %derived from Table 3a from source
N2 = 1.3; %derived from Table 3b from source
N = N1*N2; %factor of safety
N = 2; %rounded FOS

%% Converting Load
% The Capstone Report Design Constraints lists the trike should be able to
% carry a 300 lbm (300 lbf) rider.
Lo = 300; %original load, lbf
L = Lo*N; %design safe/max load (converted load once FOS applied), lbf
FCF = 4.44822; %force conversion factor, N per lbf
Lm = L*FCF; %design safe/max load (metric units), N
Lm = 2670; %rounded load, N

%% Linear Actuator Dimensions and Properties
LAs = 6; %stroke length, in
LAc = 300; %force capacity, lbf
v = 0.39; %speed (velocity), in/s
LAV = 12; %input voltage, V DC
LAI = 7.6; %current (full load), A
P = LAI*LAV; %power delivered by linear actuator, W
PCF = 745.7; %power conversion factor, W per hp
H = P/PCF; %power (English units), hp
HCF = 550*12; %power conversion factor 2, ft-lbf/s per hp & in per ft
H2 = H*HCF; %power (English units), ft-lbf/s

%% Gear Dimensions and Properties
% Gear may also be referred to as pinion.
% Gear chosen from McMaster-Carr (part number 5172T42).
% https://www.mcmaster.com/#catalog/123/1120/=16aq1sb
% Gear is "High-Load Metal Gear", steel, spur
Pd = 8; %diametral pitch, teeth/in or in^-1
Np = 16; %number of teeth_pinion
dp = Np/Pd; %pitch diameter, in
rp = dp/2; %pitch radius, in
OD = 2.25; %outer diameter, in
F = 1.5; %face width, in
PA = 20; %pressure angle, deg
% determined steel type: medium carbon, AISI 1050
% http://www.model-engineer.co.uk/forums/postings.asp?th=40868
% https://simple.wikipedia.org/wiki/Carbon_steel
% http://www.efunda.com/materials/alloys/carbon_steels/medium_carbon.cfm
% http://www.matweb.com/search/DataSheet.aspx?MatGUID=9b8279fc95c043368b0d1b8589fc0cda
% from Matweb.com "AISI 1050 Steel, as cold drawn bar, 50-75 mm (2-3 in) round"
rho = 0.284; %density, lb/in^3 (7.87 g/cc)
HB = 170; %hardness, Brinell
Sut = 84800; %tensile strength, ultimate, psi (585 MPa)
Sy = 74700; %tensile strength, yield, psi (515 MPa)
E = 29000e3; %modulus of elasticity, psi (converted from ksi) (200 GPa)
K = 23200e3; %bulk modulus, psi (converted from ksi) (160 GPa)
nu = 0.29; %Poissons ratio
G = 11600e3; %shear modulus, psi (converted from ksi) (80.0 GPa)
CTE = 6.39e-6; %coefficient of thermal expansion, in/(in-degF) (11.5e-6 m/(m-degC))
Cp = 0.116; %specific heat capacity, BTU/(lb-degF) (0.486 J/(g-degC))
k = 360; %thermal conductivity, (BTU-in)/(hr-ft^2-degF) (51.9 W/(m-K))
```

```
%% Gear Stress Analysis - Bending Stress
% source: Shigley's Mechanical Engineering Design, Tenth Edition
% specifically: Ch.14 (Spur and Helical Gears) pp725-776.
omega = (v/rp)*(1)*(60); %angular velocity, (rot/s)*(rev/rot)*(s/min), RPM
omegam = omega*(2*pi)*(1/60); %angular velocity (metric units), rad/s
                              %(rev/min)*(rad/rev)*(min/s)
Tp = H2/omegam; %torque on pinion, in-lb [EQ(13-33), p.698]
Y = 0.296; %Lewis Form Factor, since Np=16 [Table 14-2, p.730]
V = (pi*dp*omega)/12; %pitch-line velocity, ft/min (FPM) [EQ(13-34), p.699]
% Kv = (1200+V)/1200; %velocity factor [EQ(14-4b), p.731]
        %obsoleted - not preferred formula.
% Wt = (F*Y*s_all)/(Kv*Pd); %transmitted load, lbf [EX.14-1, p.732]
        %obsoleted - not preferred formula.
Wt = 33000*(H/V); %transmitted load, lbf [EQ(13-35), p.699]
Ko = 1; %overload factor [Sect(14-8), p.750]
        %Ko neglected because externally applied loads are NOT "in excess
        %of the nominal tangential load Wt in a particular application".
        %Also, from table at bottom of p.758: Power source determined to be
        %Uniform/Uniform therefore Ko=1.
Kv_Qv = 3; %quality number (worst case since not specified) [Sect(14-7), p.748]
        %Quality numbers 3 to 7 will include most commercial quality gears.
        %Quality numbers 8 to 12 are of precision quality.
Kv_B = 0.25*((12-Kv_Qv)^(2/3)); %dynamic factor constant B [EQ(14-28), p.748]
Kv_A = 50+(56*(1-Kv_B)); %dynamic factor constant B [EQ(14-28), p.748]
Kv = ((Kv_A+sqrt(V))/Kv_A)^Kv_B; %dynamic factor [EQ(14-27), p.748]
Ks = 1.192*((F*sqrt(Y)/Pd)^0.0535); %size factor [Sect(14-10)EQ(a), p.751]
        %Ks>1 so formula can be used. If Ks<1, Ks=1.
Cmc = 1; %Km factor, for uncrowned teeth [EQ(14-31), p.752]
Cpf = (F/(10*dp))-0.0375+(0.0125*F); %Km factor, for 1"<F<=17" [EQ(14-32), p.752]
Cpm = 1; %Km factor, neglected because no shaft in design [EQ(14-33), p.752]
Cma_A = 0.247; %Km factor for Cma [Table 14-9, open gearing, p.752]
Cma_B = 0.0167; %Km factor for Cma [Table 14-9, open gearing, p.752]
Cma_C = -0.765e-4; %Km factor for Cma [Table 14-9, open gearing, p.752]
Cma = Cma_A+(Cma_B*F)+(Cma_C*(F^2)); %Km factor [EQ(14-34), p.752]
Ce = 1; %Km factor, for all other conditions [EQ(14-35), p.752]
Km = 1+(Cmc*((Cpf*Cpm)+(Cma*Ce))); %load-distribution factor [EQ(14-30), p.751]
Cmf = Km; %face load distribution factor [EQ(14-30), p.751]
tR = 0.417875; %rim thickness, in. (measured in McMaster's CAD file of gear)
ht = 0.53925/2; %tooth height, in. (measured in McMaster's CAD file of gear)
mB = tR/ht; %backup ratio [EQ(14-39), p.756]
KB = 1; %rim-thickness factor, because mB>=1.2 [EQ(14-40), p.756]
mN = 1.0; %load-sharing ratio, mN=1.0 for spur gears [EQ(14-21), p.745]
Kf = 1; %fatigue stress-concentration factor [Sect(6-10), p.303]
        %dependent on notches, none accounted for: neglect.
J = Y/(Kf*mN); %AGMA bending-strength geometry factor [EQ(14-20), p.744]
        %EQ(14-20) used instead of [Fig.14-6, p.745] because Fig.14-6 did
        %not display Np=16 teeth.
s_bend = Wt*Ko*Kv*Ks*(Pd/F)*((Km*KB)/J) %sigma_bending
        %gear bending stress, lbf/in^2 (psi) [EQ(14-15), p.738]
St = (77.3*HB)+12800; %gear bending strength, psi
        %also referred to as: allowable bending stress number at 10^7
        %cycles and 0.99 reliability - obtained from [Fig.14-2, p.739].
        %Chose Grade 1 since grade unknown therefore chose worst case.
        %originally thought St value should be converted from ksi (Stx1000)
        %but this not done because of [EX(14-4), p.761] flow - left as psi.
NC = 10e4; %number of cycles desired for life goal of gear (chosen)
        %10e6 and greater cause SH_c to be less than one - cannot have.
YN = 2.3194*(NC^-0.0538); %stress-cycle factor [Fig.14-14, p.755]
        %use when 10e3 < NC < 10e6
        %used 160HB curve/equation since this was closest match to gear HB.
% YN = 1.3558*(NC^-0.0178); %stress-cycle factor [Fig.14-14, p.755]
        %use when 10e7 < NC < 10e10
        %used in [EX(14-4), p.760].
KT = 1.0; %temperature factor [Sect(14-15, p.756]
        %chosen because operating temperature < 250degF
R = 0.90; %reliability, typical, chosen because not stated (99%) [Sect(14-14), p.755]
% KR = 0.50-(0.109*(log(1-R))); %reliability factor [EQ(14-38), p.755]
        %obsoleted - a cardinal value of R was chosen/used (end of p.755).
KR = 0.85; %reliability factor [Table(14-10), p.756]
        %chosen because R is considered a cardinal value (end of p.755).
```

```
SF_b = ((St*YN)/(KT*KR))/s_bend; %AGMA factor of safety of gear in bending
        %also called a stress ratio, [EQ(14-41), p.757]
% s_bend_allow = (St/SF_b)*(YN/(KT*KR))
        %obsoleted - computation developed circular references with SF_b.
s_bend_allow1 = Sy/N %allowable bending stress #1 [Pugsley Method]
s_bend_allow2 = s_bend*SF_b %allowable bending stress #2
% nd = 3; %frequently prescribed design factor [EX(14-1), p.732]
% s_bend_allow3 = Sy/nd %allowable bending stress #3 [EX.14-1, p.732]
        %obsoleted - method not needed.
SF_b1 = s_bend_allow1/s_bend %FOS from method #1
SF_b2 = s_bend_allow2/s_bend %FOS from method #2 = SF_b
% SF_b3 = s_bend_allow3/s_bend %FOS from method #3
        %obsoleted - method not needed.
SF_b_avg = (SF_b1+SF_b2)/2 %average factor of safety for bending stress
%if FOS>1, design is safe.

%% Gear Stress Analysis - Contact Stress (Pitting Resistance)
% source: Shigley's Mechanical Engineering Design, Tenth Edition
% specifically: Ch.14 (Spur and Helical Gears) pp725-776.
CP = (1/(2*pi*((1-(nu^2))/E)))^(1/2); %elastic coefficient, sqrt(lbf/in^2)
        %from [EQ(14-13), p.736] - modified EQ(14-13) because pinion and
        %gear (rack in this case) are the same material.
CF = 1; %surface condition factor [Sect(14-9), p.750]
        %assumed 1 because no surface conditions are known.
phiN = PA; %normal pressure angle believed to be equal to
           %pressure angle (spur gear), deg
psi = 0; %helix angle, deg (0 because spur gear)
phiT = atand(tand(phiN)/cosd(psi)); %transverse pressure angle, deg [EX(14-5), p.763]
NG = Np; %number of teeth on gear, assumed equal to Np because the gear is
         %replaced by the rack in this system, where the rack is
         %dimensionally identical/equivalent to the selected pinion gear,
         %except straightened/rolled out.
mG = NG/Np; %gear speed ratio, equals 1 because the selected rack and
        %pinion teeth are dimensionally equivalent [EQ(14-22), p.746]
I = ((cosd(phiT)*sind(phiT))/(2*mN))*(mG/(mG+1)); %surface-strength
        %geometry factor, also called the pitting-resistance geometry
        %factor, for external spur gears [EQ(14-23), p.747]
s_cont = CP*sqrt(Wt*Ko*Kv*Ks*(Km/(dp*F))*(CF/I)) %contact stress, psi
        %also called pitting resistance [EQ(14-16), p.738]
Sc = (322*HB)+29100; %allowable contact stress number, psi
        %also called contact-fatigue strength at 10^7 cycles and 0.99
        %reliability. Value calculated from Grade 1 curve from
        %[Fig(14-5), p.742], assuming worst case scenario since grade
        %unknown - this was redirected from [Table(14-6), p.743] and
        %material designation (steel) and through hardened (heat treatment)
        %was chosen to be closest to this application.
ZN = 2.466*(NC^-0.056); %pitting resistance stress-cycle factor [Fig(14-15), p.755]
        %use when 10e4 < NC < 10e7 (ZN=1 at NC=10e7).
        %taken from non-nitrided trendline.
% ZN = 1.4488*(NC^-0.023); %pitting resistance stress-cycle factor [Fig(14-15), p.755]
        %use when 10e7 < NC < 10e10
        %used in [EX(14-4), p.760].
CH = 1; %hardness-ratio factor [Sect(14-12), p.753]
        %this factor is used only for the gear and equals 1 for the pinion.
SH_c = ((Sc*ZN*CH)/(KT*KR))/s_cont; %wear factor of safety [EQ(14-42), p.757]
% s_cont_allow = (Sc/SH_c)*((ZN*CH)/(KT*KR)); %gear contact endurance strength, psi
        %also referred to as the allowable contact stress [EQ(14-18), p.742]
        %obsoleted - computation developed circular references with SH_c.
        %if greater than 1, the design is safe.
s_cont_allow = s_cont*SH_c %allowable contact stress, psi
SH_c %display the wear factor of safety

%% Done.
```

Engineering

Capstone Report Approval Form

Master of Science in Engineering – MSE

Milwaukee School of Engineering

This capstone report, entitled "Design and Analysis of a Human Powered Vehicle's Frame and Seat Assistance Mechanism," submitted by the student Bradley S. Helm, has been approved by the following committee:

Faculty Advisor: _____ Date: _____

Dr. Subha K. Kumpaty, Ph.D.

Faculty Member: _____ Date: _____

Dr. Nebojsa Sebastijanovic, Ph.D.

Faculty Member: _____ Date: _____

Professor Gary Shimek, M.L.I.S.